Deep Sensing for Space-Time Doubly Selective Channels: When a Primary User Is Mobile and the Channel Is Flat Rayleigh Fading

Bin Li, Jia Hou, Xiaofan Li, *Member, IEEE*, Yijiang Nan, Arumugam Nallanathan, *Senior Member, IEEE*, and Chenglin Zhao

***Abstract*—The unrestrained mobility and dynamic spectrum sharing are considered as two key features of next-generation communications. In this paper, spectrum sensing in mobile scenarios is investigated, which faces still great challenges as both the mobile location of primary-user and fading channel will become time-variant. Such two uncertainties would arouse remarkable fluctuations in the strength of received signals, making most existing sensing schemes invalid. To cope with this exceptional difficulty, a novel paradigm, i.e., deep sensing, is designed, which estimates the time-dependent flat-fading gains and primary-user's mobile positions jointly, at the same time of detecting its emission status. All three hidden states involved by the space-time doubly selective scenario are taken into accounts. A unified dynamic state-space model is established to characterize the dynamic behaviors of unknown states, in which the time-dependent flat fading is modeled as a stochastic discrete-state Markov chain. A Bayesian approach, premised on a formulation of random finite set, is suggested to recursively estimate primary user's unknown states accompanying two others link uncertainties. In order to avoid the mis-tracking of the mobile positions, which is caused either by the incessant disappearance of primary-user or time-variant channels, an adaptive horizon expanding mechanism is also integrated. Numerical simulations validate the proposed scheme.**

***Index Terms*—Spectrum sharing, spectrum sensing, mobile PU, time-correlated flat fading, Bayesian estimation.**

I. Introduction

BY PROMOTING the spectrum utilization of authorized frequency and thereby alleviating the spectrum scarcity, dynamic spectrum sharing (DSS) provides the great promise to next-generation communications [1], which may pave a way for the development of new wireless services without allocating extra frequency [2], [3]. For the emerging indoor applications, e.g., the license assisted access (LAA) to the WiFi band discussed in LTE-U [3], [4], a primary user (PU) can be a smartphone or a personal digital assistant (PDA) that will be move around in the local region. For other outdoor applications, e.g., the cognitive wireless sensor networks (C-WSN), the PU may be a mobile device occupying the primary band. It is recognized that, except for the occupancy status of primary band which is usually acquired via spectrum sensing techniques, the mobile locations of PU and the time-dependent channels will be of great significance to the performance enhancement of cognitive radios (CRs) [5], [17]. When it comes to identifying PU's unknown states in complex electromagnetic environments, however, such two participating random components (i.e., the mobility of PU's locations and the variation of fading channels) will bring great challenges to the practical deployment of spectrum sensing.

Spectrum sensing, i.e., the real-time monitoring of the presence or absence of PU, is formulated essentially as a *detection* or hypothesis-test problem [7]. Since the advent of CRs, various sensing algorithms of different advantages and requirements have been developed [7]–[10]. Most traditional schemes, e.g., energy detector (ED) [11], [12], unfortunately are vulnerable to information uncertainties, e.g., the large-scale *space-varying* path loss or meso-scale *time-varying* fading channel. As suggested by [12], [13], the fading effect, given the *a priori* probability density function (PDF), will be marginalized out. By focusing simply on its instantaneous random behavior, this commonly used technique, however, ignores the correlation of time-varying flat fading [13]. Thus, it will be less competitive, in consideration of tracking time-dependent channels and further exploiting the underlying dynamic property. As far as the space-time doubly selective channels are concerned, i.e., with a mobile PU and variant channel fading, realistic observed signals will show remarkable fluctuations, which makes most existing sensing schemes invalid.

The tracking of PU's locations, on the other hand, belongs to another parameters *estimation* issue. Traditional techniques include the externally aided positioning and the passive localization [14]. The first approach relies on specific external systems, e.g., global positioning system (GPS) or ultra-wideband [15]. The second method, in contrast, estimates the mobile positions by exploiting the information of observations, e.g., the re-

Manuscript received August 21, 2015; revised January 08, 2016; accepted February 11, 2016. Date of publication March 02, 2016; date of current version May 18, 2016. The associate editor coordinating the review of this manuscript and approving it for publication was Dr. Pengfei Xia. This work is supported by Natural Science Foundation of China (NSFC) under Grants 61471061 and the Fundamental Research Funds for the Central Universities under Grant 2014RC0101.

B. Li, Y. J. Nan and C. Zhao are with the School of Information and Communication Engineering (SICE), Beijing University of Posts and Telecommunications (BUPT), Beijing 100876, China (e-mail: stonebupt@gmail.com).

J. Hou is with School of Electronic and Information Engineering, Soochow University, Suzhou 215006, China (e-mail: houjia@suda.edu.cn).

X. Li is with the State Radio Monitoring Center Testing Center (SRTC), Beijing 100041, China (e-mail: lixiaofan@srtc.org.cn).

A. Nallanathan is with the Department of Informatics Engineering, King's College London, London, WC2R2LS, U.K. (e-mail: nallanathan@ieee.org).

Color versions of one or more of the figures in this paper are available online at http://ieeexplore.ieee.org.

Digital Object Identifier 10.1109/TSP.2016.2537276

1053-587X © 2016 IEEE. Personal use is permitted, but republication/redistribution requires IEEE permission.
See http://www.ieee.org/publications_standards/publications/rights/index.html for more information.

ceived signal strength (RSS) [16] or the time of arrivals (ToAs) (or maybe the hybrid information) [17]. It is noteworthy that, for CR applications, usually most external systems will be impractical. Moreover, the localization of a mobile PU has to be accomplished in a non-coordinated manner and, thus, the available information will be very limited (e.g., only RSS may be used). The innate reason is that a PU endowed with the absolute priority (on its authorized spectrum) is not bound to accommodate the inferior secondary users (SUs).

For a space-time doubly selective scenario, one has to deal with a more complicated *mixed* detection and estimation problem. The principal challenge is that the detection process (of PU's emission status) and the other estimation process (of two related link uncertainties) will be mutually interrupted. Unlike traditional joint estimation and detection problem [18], the RSS emitted by a PU will *disappear* randomly attributed to the dynamic switching of its occupancy status, making the acquisition of PU's moving positions and time-dependent channels even tough. To be specific, an erroneous PU's state will misguide the inference (or estimation) of its mobile positions accompanying the fading channels, which, in turns, will definitely harass the next round of detection. Most existing schemes, designed either for *pure* sensing or estimating problems, fail to take such coupling and transitive interruptions into account, which may become less attractive to the spectrum-location awareness application. For example, the Cramér-Rao bound of PU localization is studied [19], which, yet of theoretical significance, did not consider the incessant disappearance of PU's RSS and time-dependent fading channels.

Spectrum sensing under time-dependent fading channels is firstly investigated in [13], where the *fixed* path-loss (i.e., with a non-mobile PU) is assumed. The sensing algorithm with a mobile PU is then studied [20], which, however, considers only a *static* Gaussian channel and may be impractical to many applications. In the face of more realistic time-dependent fading, existing schemes will be infeasible due to the further coupling interaction between two unknown link states. For example, a direct application of the method in [20] to the new scenario will lead to significant estimation errors, e.g., when localizing a mobile PU based on inaccurate fading channel, or vice versa. To the best of our knowledge, spectrum sensing, in the context of the space-time doubly selective channels, has not been virtually reported in the open literature. In the investigation, a general deep sensing (DS) framework is suggested for more challenging scenarios. To sum up, the main contributions are summarized to the following three-folds.

1. An extended DS paradigm is proposed for the *mixed* estimation of PU's emission states and another two dynamic uncertainties. Differentiated from classical sensing schemes ignoring a mobile PU and the flat-fading effect [7]–[11], or existing localization techniques without considering PU's switching states and time-variant channels [17], [18], the new framework will take thoroughly the destructive interruption from the PU's incessant absence into the blind tracking of its positions and time-varying fading channels.
2. A general dynamic state-space model (DSM) is established to characterize the DS process in space-time doubly selective fading channels. In contrast to other traditional sensing formulations or localization models, in the new DSM the time-varying fading channels and PU's moving positions are treated as two hidden states to be estimated, other than the unknown emission status of PU. The mutually interrupting relationship, as a consequence, will be fully embodied.
3. A recursive algorithm is designed to realize spectrum sensing under both the time-variant fading effect accompanying the PU's mobility, which, unfortunately, seems to be beyond the capability of other existing schemes [7], [9]. The complex DS process, aiming to acquiring another two informative link uncertainties, is modeled as a Bernoulli random finite set (RFS). A Bayesian approach is then suggested, in which a sequential importance sampling (SIS) method is adopted. The non-analytical posterior densities are approximated numerically, and the PU's state accompanying two link states are recursively derived. By updating the degree uncertainty, an adaptive horizon expanding (AHE) mechanism is further integrated, which could avoid the mis-tracking despite the incessant disappearance of PU's signals.

The sensing performance, accompanying the estimation performance of two link uncertainties, are studied based on numerical simulations. It is shown that, no matter what the PU's state is, both time-varying fading channels and PU's mobile locations can be tracked. Based on the recovered two informative link states, the promising sensing performance can be achieved in space-time doubly selective fading channels. Note that, the estimated fading states and PU's locations, as the extra gifts of sensing process, will be of great potentiality to CRs' performance enhancement [17], e.g., interference control and resource allocation. The extended DS scheme, therefore, provides a promising approach for DSS-based next-generation communications.

The rest of the article is arranged as follows. In Section II, a general DSM is formulated to characterize the spectrum-location awareness problem under time-dependent fading conditions. A recursive Bayesian algorithm is designed in Section IV, which acquires PU's emission states by inferring its locations and fading channels simultaneously. A promising AHE is also integrated to avoid the mis-tracking of a mobile PU. Simulations are provided in Section V. Finally, we conclude this study in Section VI.

The notations used by this work are summarized as follows: the $n \times 1$ dimensional vector is denoted by $\mathbf{x}_{n\times 1}$; the $M \times N$ matrix is $\mathbf{X}_{M\times N}$; $\boldsymbol{\mathcal{F}}$ denotes a random finite set and $|\boldsymbol{\mathcal{F}}|$ is its cardinality; $\mathcal{A}^{n_x}$ denotes a discrete state space of n_x dimensions; $\mathbb{R}^{n_x\times 1}$ is the real-valued space of n_x dimensions; $\mathbb{N}$ is the 1-dimension integer space. $\|\mathbf{x}\|_2^2 = \sum_n x^2(n)$ is the l_2-norm of vector $\mathbf{x}$. $(\cdot)^T$ denotes the transpose. $x_{0:n} \triangleq \{x_0, x_1, x_2, \ldots, x_n\}$ is the variable trajectory till the nth time index. $\mathsf{E}(\cdot)$ denotes the ensemble average, and $\mathsf{V}(\cdot)$ is the variance.

II. System Model and Problem Formulation

For the spectrum-location awareness application, we consider a cooperative sensing scenario. It is assumed that the large-scale

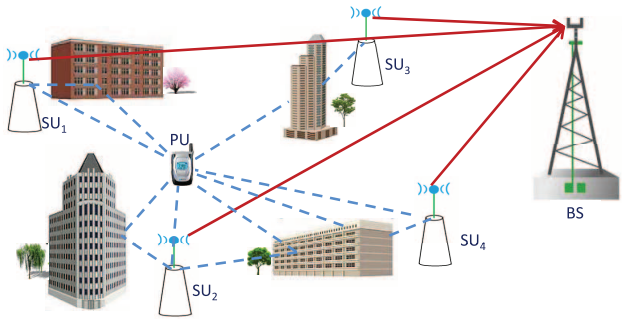

Fig. 1. A outdoor DS scenario under space-time doubly selective channels with $K = 4$ collaborative SUs. The *large-scale* pass-loss is determined by the geographic distance between the mobile PU and SUs, while the fading effect is related with local environment. The *dash* lines denote the first-phase sensing procedure, while the *solid* lines account for the second-phase report process.

path-loss is determined by the geographic distance between a mobile PU and the rth SU, while the flat-fading is aroused by the superposition of independent reflections, as illustrated by Fig. 1. For simplicity, here R SU nodes are assumed to be located on a 2-D grid. The position of the rth SU node, denoted by $\mathbf{l}_r^{SU} = [x_r', y_r']^T$, is known by the data-center (maybe an outdoor base-station or the indoor access-point) as *a priori*.

At the discrete time n, the rth SU will obtain the local observation $z_{n,r}$. All R SU nodes will then forward the observations toward to a data center, which will estimate the fading gains and PU's emission status s_n accompanying its position (x_n, y_n), relying on the received observation vector $\mathbf{z}_n = [z_{n,1}, z_{n,2}, \ldots, z_{n,R}]^T$.

A. Single Model

A new DSM is formulated to characterize the above spectrum-location awareness scenario, i.e.,

$$s_n = S(s_{n-1}), \tag{1}$$
$$\boldsymbol{\alpha}_n = A(\boldsymbol{\alpha}_{n-1}), \tag{2}$$
$$v_n = V(v_{n-1}, u_{n,1}), \tag{3}$$
$$\theta_n = \Theta(v_{n-1}, u_{n,1}), \tag{4}$$
$$\mathbf{l}_n = L(\mathbf{l}_{n-1}, v_n, \theta_n), \tag{5}$$
$$z_{n,r} = Z(\mathbf{l}_n, \boldsymbol{\alpha}_n, s_n, w_{n,r}). \tag{6}$$

Here, (1)–(5) are referred to dynamic equations, while (6) accounts for the measurement equation.

1) The first dynamic function $S(\cdot) : \mathbb{Z}^1 \mapsto \mathbb{Z}^1$, which is non-analytical and specified by a group of transitional probabilities, characterizes the stochastic switching of PU's emission states $s_n \in \mathcal{S} = \{0, 1\} \subset \mathbb{Z}^1$ from the $(n-1)$th to nth time slot.
2) The second dynamic function $A(\cdot) : \mathbb{R}^{K\times 1} \mapsto \mathbb{R}^{K\times 1}$ depicts the transitions of fading channels $\boldsymbol{\alpha}_n = [\alpha_{n,1}, \alpha_{n,2}, \ldots, \alpha_{n,R}]^T$. Here, each fading gain $\alpha_{n,r}$ is assumed to follow a discrete-states Markov chain (DSMC) of one order. Note that, this analysis will focus primarily on the *multiplicative* time-varying flat-fading, while the frequency-selective multipath effect is ignored.
3) Another two dynamic functions, $V(\cdot) : \mathbb{R}^1 \mapsto \mathbb{R}^1$ and $\Theta(\cdot) : \mathbb{R}^1 \mapsto \mathbb{R}^1$, specifies the random evolutions of PU's moving speed v_n and orientation θ_n, which are driven respectively by two random noises $u_{n,1}$ and $u_{n,2}$.
4) The dynamic function $L(\cdot) : \mathbb{R}^2 \mapsto \mathbb{R}^1$ gives the time variations of PU's locations $\mathbf{l}_n = [x_n, y_n]^T$.
5) The measurement function $Z(\cdot) : \mathbb{R}^M \mapsto \mathbb{R}^2$ describes the coupling relationship between three hidden states (i.e., $s_n, \alpha_{n,r}$ and $\mathbf{l}_n$) and the observation $z_{n,r} \subset \mathbb{R}^1$. The background noise of the mth sample of the nth slot, denoted by $w_n(m) \subset \mathbb{R}^1$, is assumed to be the independent and identically distributed (i.i.d) zero-mean additive white Gaussian noise (AWGN) with a variance σ_w^2, i.e., $w_n(m) \sim \mathcal{N}(0, \sigma_w^2)$, which keeps independent of three hidden states (i.e., $s_n, \alpha_{n,r}$ and $\mathbf{l}_n$).

Without losing generality, we consider the sensing-transmission slot with a duration of $T_F = 2$ ms. Assume the relative displacement of a PU device is about 0.008 m among two sensing-transmission slots, then its mobile speed will be $v = 4$ m/s (e.g., a moving human). Taking the carrier frequency of $f_c = 2.4$ GHz for example, the maximum Doppler frequency $f_d = \frac{v \times f_c}{c}$ will be 32 Hz, where $c = 3 \times 10^8$ m/s is the velocity of light. In this case, the static length of flat-fading channel is about $L \simeq \lfloor \frac{1}{f_d T_F} \rfloor = 15$. That is, the fading gain will remain temporarily unchanged in 15 successive sensing-transmission slots, while it may vary in the next L slots. For a smaller mobile speed, e.g., $v = 1$ m/s, then the static length of flat-fading channel will be even longer, i.e., $L \simeq 62$. In the following analysis, three assumptions are made to the established DSM.

1) The PU's emission state s_n is assumed to be quasi-static. If H_0 corresponds to a hypothesis in the absence of PU's signals and H_1 accounts for the presence of PU, then either H_1 or H_0 will be unchanged during one sensing slot T_s.
2) The slowly varying fading channel is concerned. In this case, each fading gain $\alpha_{n,r}$ will remain invariant during L successive slots, but it will changed in the next L slots. As shown, the static length L is practically related with the maximum Doppler shift f_d, i.e., $LT_F \simeq 1/f_d$. Besides, it is assumed that R fading gains of different PU-SU links evolve independently.
3) The PU is assumed to move slowly (e.g., $v < 4$ m/s). Thus, the mobile position $\mathbf{l}_n = [x_n, y_n]^T$ will remain invariant within one sensing slot (recall a slot is very short, e.g., 2 ms). In other words, $\mathbf{l}_n$ is independent of different sample index m of the nth sensing slot.

Next, we will elaborate on each state/observation equation.

B. PU's Emission States

The evolution of PU's emission states is typically characterized by a two-state Markov transition process $\mathcal{S} = \{S_0, S_1\}$ [12], [22]. In practice, the dynamical transitions of PU's states may keep invariant for a given application in all the time (or, at least, in a long period). So, the transitional probability matrix (TPM) of PU's emission states is given by:

$$\boldsymbol{\Pi} = \begin{bmatrix} (1-p_b) & p_b, \\ (1-p_s) & p_s. \end{bmatrix}, \tag{7}$$

where the *survival* probability p_s is defined as:

$$p_s := \Pr\{s_{n+1} = 1 | s_n = 1\}, \tag{8}$$

and the birth probability p_b as:

$$p_b := \Pr\{s_{n+1} = 1 | s_n = 0\}. \tag{9}$$

C. Time-Varying Fading

The time-varying flat fading channel, as the common feature of next-generation communications enabling unrestrained mobility [3], [5], is taken into account. The transitional behavior of time-correlated channel is modeled as a DSMC [12], [23], [25], which is shown to coincide with the dynamic nature of time-varying channel and also match existing statistical models (e.g., Clarke's model) well [23], [25]. For simplicity, here an indecomposable DSMC is studied.

For the non-coherent RSS observation, it is noteworthy that the channel phase will be insignificant to the DS process [12], whilst the channel gain with a specific statistic distribution, e.g., Rayleigh fading [24], is of crucial importance. In the DMSC, the rth nonnegative fading gain $\alpha_{n,r} \in (0, +\infty)$ will be divided to K non-overlapping regions, denoted by $\mathbb{V}_r$. If two partition bounds are specified by $v_{0,r} = 0$ and $v_{K,r} = \infty$, respectively, then we have:

$$\mathbb{V}_r = \{ (v_{0,r}, v_{1,r}), [v_{1,r}, v_{2,r}), \ldots, [v_{K-1,r}, v_{K,r})\}. \quad (10)$$

Thus, the time-varying fading channel will be represented by a group of discrete states, i.e., $\mathcal{A}_r \triangleq \{\mathrm{A}_{1,r}, \mathrm{A}_{2,r}, \ldots, \mathrm{A}_{k,r}\}$. Each gain $\alpha_{n,r} = \mathrm{A}_{k,r} \in \mathcal{A}_r, k \in [0, 1, \ldots, K-1]$ is viewed as the output of a specific DSMC [25]. The stationary probability of the rth fading gain is denoted by $\boldsymbol{\rho}_r = [\rho_{0,r}, \rho_{1,r}, \ldots, \rho_{K-1,r}]^T$ with $\rho_{k,r} \triangleq \Pr(\alpha_{n,r} = \mathrm{A}_{k,r})$. Then, we have $\mathbf{P}_r^T \boldsymbol{\rho}_r = \boldsymbol{\rho}_r$ for the assumed indecomposable DSMC, where $\mathbf{P}_{K\times K,r} = \{\rho_{k_1 \to k_2, r}, k_1, k_2 \in [0, 1, \ldots, K-1]\}$ denotes the TPM of fading gains and each element $\rho_{k_1 \to k_2, r}$ specifies the transitional probability from the state k_1 at time $(n'-1)$ to the state k_2 at time n'.

$$\rho_{k_1 \to k_2, r} = \Pr\left(\alpha_{n',r} = \mathrm{A}_{k_2,r} | \alpha_{n'-1,r} = \mathrm{A}_{k_1,r}\right). \quad (11)$$

In practice, the above transitional probabilities are usually ergodic and stationary [12], [23], [26]. That means the prior densities $\rho_{k_1 \to k_2, r}$ are independent of the transitional time $n' = \lfloor n/L \rfloor$ of fading channels.

Suppose the statistical PDF of the Rayleigh fading is denoted by $f(\alpha)$, then the steady probabilities of the fading gain $\alpha_{n,r}$ residing in the kth region (i.e., A_k) are:

$$\rho_{k,r} = \int_{v_{k,r}}^{v_{k+1,r}} f(\alpha_{n,r}) d\alpha_{n,r},$$
$$\mathrm{A}_{k,r} = \frac{1}{\rho_{k,r}} \int_{v_{k,r}}^{v_{k+1,r}} \alpha_{n,r} f(\alpha_{n,r}) d\alpha_{n,r}. \quad (12)$$

With an equiprobable partition rule, i.e., $\rho_{k,r} \triangleq 1/K$, the partitioning bounds will be derived via $v_{k,r} = -2\sigma^2 \times \ln(1 - k/K)$ [23]. So, $\rho_{k_1 \to k_2, r}$ is evaluated via:

$$\begin{aligned}\rho_{k_1 \to k_2, r} &= \Pr\left\{ \alpha_{n',r} \in [v_{k_1,r}, v_{k_1+1,r}) \middle| \, \alpha_{n'-1,r} \in [v_{k_2,r}, v_{k_2+1,r}) \right\} \\ &= \frac{1}{\rho_{k,r}} \int_{v_{k_2,r}}^{v_{k_2+1,r}} \int_{v_{k_1,r}}^{v_{k_1+1,r}} f(\alpha_{n'-1,r}, \alpha_{n',r}) d\alpha_{n'-1,r} d\alpha_{n',r}, \end{aligned} \quad (13)$$

where $f(\alpha_{n'-1,r}, \alpha_{n',r})$ is the bi-variate Rayleigh joint PDF [26].

For simplicity, the 1st-order DSMC is assumed, which is proven to be applicable in most slowly varying flat-fading environments [25]. The current fading state, accordingly, will keep independent of all other past and future fading states with a standoff distance larger than 1, i.e., $\rho_{k_1 \to k_2, r} = 0$ for $|k_1 - k_2| > 1$. Thus, the TPM $\mathbf{P}_{K\times K,r}$ of DSMC is simplified to a *tridiagonal* matrix, i.e., the nonzero elements exist only on the main diagonal and the first diagonal below/above this main diagonal.

For convenience, R PU-SU links are *homogeneous* and the fading properties will be the same, i.e., $\mathbf{P}_{K\times K,r} = \mathbf{P}_{K\times K}$, and then the subscript r may be dropped from the above transitional probabilities. In practice, the transitional probabilities $\rho_{k_1 \to k_2}$ will be evaluated by a numerical method [23], [25] premised on the level crossing rate (LCR) N_k, which accounts for the number of times per second that the fading amplitude crosses v_k in a downward direction. For the assumed Rayleigh fading, we have:

$$N_k = \frac{\sqrt{2\pi} f_D v_k}{\sigma} \times \exp\left(-v_k^2/\sigma^2\right). \quad (14)$$

Relying on the conception of LCR, the transitional probabilities will be approximated by $\rho_{k_1 \to k_2} \simeq N_{k_2}/R_{k_1}$. Here, $R_{k_1} = \rho_{k_1}/T_F$ is the average number of sensing slots per second in the state k_1, and $T_F > T_s$ denotes the duration of the sensing-transmitting slot.

D. PU's Locations

A flexible mobility formulation, i.e., the Gauss-Markov mobility (GMM) model, is studied, which has been widely used in mobile ad-hoc networks [27], [28]. A similar parametric model may be adapted for mobile cellular scenarios [28]. The parameters would be extracted from various application scenarios, e.g., indoor/outdoor, human/vehicle.

Given the updated PU's speed and orientation, the dynamic positions $\mathbf{l}_n$ will be evolved randomly according to:

$$\begin{aligned}\mathbf{l}_n &= \mathbf{l}_{n-1} + \Delta(v_n, \theta_n) \\ &= [x_{n-1} \ y_{n-1}]^T + v_n \times [\cos(\theta_n) \ \sin(\theta_n)]^T, \end{aligned} \quad (15)$$

where x_n and y_n denote the horizon and vertical positions of a mobile PU at the nth discrete time.

In order to fully characterize the mobility displacement $\Delta(v_n, \theta_n)$, the dynamic behaviors of both PU's moving speed and orientation are assumed to follow the random walking (or Brownian motion). That is, given the speed v_{n-1} and the moving orientation θ_{n-1} of the previous $(n-1)$th discrete time, then these two random states of time n will be derived by:

$$v_n = v_{n-1} + u_{n,1}, u_{n,1} \sim \mathcal{N}(0, \sigma_v^2), \quad (16)$$
$$\theta_n = \theta_{n-1} + u_{n,2}, u_{n,2} \sim \mathcal{E}(0, \sigma_\theta^2), \quad (17)$$

where σ_v^2 and σ_θ^2 denote two random variances of PU's speed and orientation, respectively. In the above GMM model, a Gaussian random noise, i.e., $u_{n,1} \sim \mathcal{N}\left(0, \sigma_v^2\right)$, serves as the driven-input of speed; whilst the other exponential noise $u_{n,2} \sim \mathcal{E}\left(0, \sigma_\theta^2\right)$ is adopted as the orientation driven-input. Note that, in practice, however the estimation scheme will be adapted of specific GMM models.

E. Observations

As mentioned, the RSS-based observation is considered, which is easy to implement and, therefore, has been widely

suggested [7]–[10], [12]. Traditionally, the sensing procedure is formulated as a two-hypothesis problem:

$$z_{n,r} \triangleq \sum_{m=1}^{M}\left[\alpha_{n,r}\sqrt{E_s}b_n(m)d_{n,r}^{-\epsilon/2}\delta(s_n-S_1)+w_n(m)\right]^2$$
$$=\begin{cases}\sum_{m=1}^{M} w_n^2(m), & H_0, \quad (18a)\\ \sum_{m=1}^{M}\left[\alpha_{n,r}\sqrt{E_s}b_n(m)d_{n,r}^{-\epsilon/2}+w_n(m)\right]^2, & H_1, \quad (18b)\end{cases}$$

where $z_{n,r}$ represents the RSS of the nth time from the rth SU device; $d_{n,r}=||\mathbf{l}_n-\mathbf{l}_r^{SU}||_2=\sqrt{(x_n-x_r)^2+(y_n-y_r)^2}$ denotes the geographic distance between the rth SU and the PU; ϵ is the attenuation constant which is typically larger than 2 and $d_{n,r}^{\epsilon}$ thereby gives the path-loss; $\alpha_{n,r}$ is the fading gain of the rth SU; M denotes the samples size. $b_n(m)$ represent PU's information symbols. For simplicity, the real-valued binary phase shift keying (BPSK) signal is assumed, e.g., $b_n(m)\in\mathcal{B}=\{+1,-1\}$. It is shown that, given the RSS-based non-coherent scheme, the generalization to unknown modulated signals (e.g., complex signals) is straightforward [12], [13].

Conditioned on the PU's state s_n and two others link states, i.e., the geographic distances $d_{n,r}$ and the fading gains $\alpha_{n,r}$, the likelihood function $\varphi(z_{n,r}|d_{n,r},\alpha_{n,r},s_n)$ follows the central chi-square distribution with the degrees of freedom (DoF) of M under H_0, and a non-central chi-square distribution with M degrees under H_1. The non-central parameter is $\varrho_{n,r}=\sum_{m=1}^{M}\left|\alpha_{n,r}d_{n,r}^{-\epsilon/2}\sigma_b\right|^2$, where $\sigma_b^2=\mathsf{E}_{\mathcal{B}}\{b_n^2(m)\}\triangleq E_s$.

For the i.i.d noise, the likelihoods are approximated by the Gaussian distributions according to the central limit theorem (CLT), when the sample size M is lager (e.g., $M\geq 50$), i.e.,

$$\varphi(\mathbf{z}_n|\mathbf{l}_n,\boldsymbol{\alpha}_n,s_n=1)=\prod_{r=1}^{R}p(z_{n,r}|d_{n,r},\alpha_{n,r},s_n=1)$$
$$\sim\prod_{r=1}^{R}\mathcal{N}\left(\mathsf{E}\{z_{n,r}|\mathbf{l}_n,\alpha_{n,r},s_n=1\},\mathsf{V}\{z_{n,r}|\mathbf{l}_n,\boldsymbol{\alpha}_n,s_n=1\}\right), \quad (19)$$

$$\varphi(\mathbf{z}_n|\mathbf{l}_n,\boldsymbol{\alpha}_n,s_n=0)=\prod_{r=1}^{R}p(z_{n,r}|s_n=0)$$
$$\sim\prod_{r=1}^{R}\mathcal{N}\left(\mathsf{E}\{z_{n,r}|s_n=0\},\mathsf{V}\{z_{n,r}|s_n=0\}\right), \quad (20)$$

where the means and variances are:

$$\mathsf{E}\{z_{n,r}|\mathbf{l}_n,\alpha_{n,r},s_n=1\}=M\times\left(E_s\alpha_{n,r}^2/\,d_{n,r}^{\epsilon}+\sigma_w^2\right),$$
$$\mathsf{V}\{z_{n,r}|\mathbf{l}_n,\alpha_{n,r},s_n=1\}=M\times\left(E_s\sigma_w^2\alpha_{n,r}^2/\,d_{n,r}^{\epsilon}+4\sigma_w^4\right),$$
$$\mathsf{E}\{z_{n,r}|s_n=0\}=M\times\sigma_w^2,$$
$$\mathsf{V}\{z_{n,r}|s_n=0\}=4M\times\sigma_w^4.$$

III. Deep Sensing

A. MAP Estimation

Without taking additional link uncertainties, e.g., unknown PU's positions and dynamic fading channels, traditionally the spectrum sensing is realized via the well-known Neyman-Pearson (NP) criterion [7]–[11], [29]. In the investigation, a novel Bayesian inference approach is designed, which, in contrast, acquires both PU's unknown emission states and its moving positions accompanying time-correlated fading gains.

Based on the formulated DSM, the maximum *a posteriori* (MAP) criterion is applied. That is, the hidden states are estimated by maximizing the joint posterior density, i.e.,

$$(\hat{\mathbf{l}}_n,\hat{\boldsymbol{\alpha}}_n,\hat{s}_n)=\arg\max_{\mathbf{l}_n\in\mathbb{R}^2,\boldsymbol{\alpha}_n\in\mathcal{A}^R,s_n\in\mathcal{S}}p(\mathbf{l}_{1:n},\boldsymbol{\alpha}_{1:n},s_{1:n}|\mathbf{z}_{1:n}), \quad (21)$$

where $s_{1:n}\triangleq\{s_1,\ldots,s_n\}$ denotes the trajectory of PU's emission states until the nth time slot. Similarly, $\mathbf{l}_{1:n},\boldsymbol{\alpha}_{1:n}$ and $\mathbf{z}_{1:n}$ denote three trajectories of PU's positions, time-varying fading gains and RSS observations, respectively.

For convenience, the hidden states are represented by a single state-vector, i.e., $\mathbf{S}_n\triangleq\{s_n,\mathbf{l}_n,\boldsymbol{\alpha}_n\}\in\mathbb{Z}^1\times\mathbb{R}^2\times\mathcal{A}^R\subset\mathbb{R}^{R+3}$. In order to derive the posterior density sequentially, a two-step Bayesian scheme [30], i.e., first predicting and then updating, is suggested, see (22)–(23) at the bottom of the page.

Here, $p_{n-1|n-1}(\mathbf{S}_{n-1}|\mathbf{z}_{1:n-1})$ denotes the *a posteriori* density of the time $n-1$. The initial distribution $p(\mathbf{S}_0)$ is assumed to be known as *a priori*. The one-step prediction $p_{n|n-1}(\mathbf{S}_n|\mathbf{z}_{1:n-1})$, as in (22), is obtained via the Chapman-Kolmogorov equation. Then, the updated posterior density, as in (23), is recursively computed on new measurements $\mathbf{z}_n$ via the Bayesian rule.

Although providing a conceptional framework of statistical inference, the existing Bayesian approach of (23)-(24) may be infeasible in the mixed sensing and positioning problem. This is attributed to the mutual interruptions between the detecting of PU emission states and the tracking of two link uncertainties. 1) In dynamic CR scenarios, as indicated, the PU's emission signals will be disappearing incessantly. Both the dynamic distance $d_{n,r}$ and fading gains $\alpha_{n,r}$ will vanish from the observation $z_{n,r}$ when a PU turns off (i.e., H_0), leading to the *likelihood dispersion* problem which renders the Bayesian estimation/inference (of either PU's positions or time-varying fading channels) a very tough work. 2) Without deterministic PU's positions and fading gains, the detection of PU states, as a coupling result, may be also erroneous due to the resulting uncertainties.

$$p_{n|n-1}(\mathbf{S}_n|\mathbf{z}_{1:n-1})=\int_{\mathbf{S}_{n-1}\in\mathbb{R}^{R+3}}\phi_{n|n-1}(\mathbf{S}_n|\mathbf{S}_{n-1})p_{n-1|n-1}(\mathbf{S}_{n-1}|\mathbf{z}_{1:n-1})d\mathbf{S}_{n-1}, \quad (22)$$

$$p_{n|n}(\mathbf{S}_n|\mathbf{z}_{1:n})=\frac{\varphi_n(\mathbf{z}_n|\mathbf{S}_n)p_{n|n-1}(\mathbf{S}_n|\mathbf{z}_{1:n-1})}{\int_{\mathbf{S}_n\in\mathbb{R}^{R+3}}\varphi_n(\mathbf{z}_n|\mathbf{S}_n)p_{n|n-1}(\mathbf{S}_n|\mathbf{z}_{1:n-1})d\mathbf{S}_n}. \quad (23)$$

B. Bernoulli Random Finite Set

With a mixed objective of simultaneous detection and estimation, traditional formulations (i.e., two hypothesis-test) may become inadequate in the context of DS. In this analysis, the dynamic behavior of all hidden states ($s_n, \mathbf{l}_n$ and $\boldsymbol{\alpha}_n$) will be characterized by one unified random process $\boldsymbol{\mathcal{F}}$, i.e., RFS [31]–[33].

1) Cardinality of RFS: An RFS is a special set containing many random variables, and its cardinality (i.e., the number of variables) will changes also with time [32]. For an RFS, the random cardinality distribution $\kappa(D) = \Pr\{|\boldsymbol{\mathcal{F}}| = D\}(D \in \mathbb{N})$ is usually vital. For the DS scenario with a mobile PU, the cardinality will be binary (i.e., $D = 0$ or $D = 1$), indicating the absence or existence of PU's signal. Thus, we have $|\boldsymbol{\mathcal{F}}| \in \{0, 1\}$ and $\kappa(D)$ is a Bernoulli distribution, i.e.,

$$\kappa(D) = \begin{cases} 1-q, & \text{if } |\boldsymbol{\mathcal{F}}_n| = 0 \text{ or } H_0, \quad (24a) \\ q, & \text{if } |\boldsymbol{\mathcal{F}}_n| = 1 \text{ or } H_1. \quad (24b) \end{cases}$$

That is, the formulated Bernoulli RFS will either be empty in the event of H_1, i.e., $\boldsymbol{\mathcal{F}}_n = \varnothing$, or have a single element $\boldsymbol{\mathcal{F}}_n = \{\mathbf{l}_n, \boldsymbol{\alpha}_n\}$ in the case of H_1. From (24), the prior probabilities of two events are given by $1-q$ and q, respectively. In the presence of PU's signal, i.e., $|\boldsymbol{\mathcal{F}}_n| = 1$, the associative random state is $\{\mathbf{l}_n, \boldsymbol{\alpha}_n\} \in \mathbb{R}^2 \times \mathcal{A}^R \subset \mathbb{R}^{2+R}$.

2) PDF of RFS: According to the Mahler's theorem [31], for a general RFS $|\boldsymbol{\mathcal{F}}_n| = D$ with a group of joint distributions $p(\mathbf{x}_1, \ldots, \mathbf{x}_D)(\mathbf{x}_D \in \mathbb{R}^{2+R})$, a statistical PDF is defined as:

$$p\left(\boldsymbol{\mathcal{F}}_n = \{\mathbf{x}_1, \ldots, \mathbf{x}_D\}\right) = D!\kappa(D)p(\mathbf{x}_1, \ldots, \mathbf{x}_D). \quad (25)$$

Obviously, $p(\boldsymbol{\mathcal{F}}_n)$ can be treated as a PDF, as the set integration on $\boldsymbol{\mathcal{F}}_n$ (note that rather than the distribution marginalization) results in $\int_{\boldsymbol{\mathcal{F}}_n} p(\boldsymbol{\mathcal{F}}_n)\delta\boldsymbol{\mathcal{F}}_n \equiv 1$.

As seen, the state associated with the active PU, i.e., $|\boldsymbol{\mathcal{F}}_n| = D = 1$, will involves two terms, i.e., the PU's moving position $\mathbf{l}_n$ and the time-varying fading state $\boldsymbol{\alpha}_n$. Replacing (24) into (25), the FISST PDF will be re-formatted as:

$$p(\boldsymbol{\mathcal{F}}_n) = \begin{cases} 1-q, & \text{if } \boldsymbol{\mathcal{F}}_n = \varnothing, \quad (26a) \\ q \times p_{n|n}(\boldsymbol{\mathcal{F}}_n = \{\mathbf{l}_n, \boldsymbol{\alpha}_n\}), & \text{if } |\boldsymbol{\mathcal{F}}_n| = 1. \quad (26b) \end{cases}$$

It is noteworthy that, for this Bernoulli RFS, we have $p(\boldsymbol{\mathcal{F}}_n) = 0$ if the cardinality D is larger than 1.

3) Dynamics of RFS: It follows from (11) and (15) that, involving two independent hidden sub-states $\mathbf{l}_n$ and $\boldsymbol{\alpha}_n$, the RFS $\boldsymbol{\mathcal{F}}_n$ follows a 1st-order Markov process and the prior transitional probabilities are given by:

$$\phi_{n|n-1}(\boldsymbol{\mathcal{F}}_n|\varnothing) = \begin{cases} 1-p_b, & \text{if } \boldsymbol{\mathcal{F}}_n = \varnothing, \quad (27a) \\ p_b b_{n|n-1}(\mathbf{l}_n, \boldsymbol{\alpha}_n), & \text{if } \boldsymbol{\mathcal{F}}_n = \{\mathbf{l}_n, \boldsymbol{\alpha}_n\}, \quad (27b) \end{cases}$$

and

$$\phi_{n|n-1}(\boldsymbol{\mathcal{F}}_n|\{\mathbf{l}_n, \boldsymbol{\alpha}_n\}), = \begin{cases} 1-p_s, & \text{if } \boldsymbol{\mathcal{F}}_n = \varnothing, \quad (28a) \\ p_s \varpi_{n|n-1}(\mathbf{l}_n, \boldsymbol{\alpha}_n|\mathbf{l}_{n-1}, \boldsymbol{\alpha}_{n-1}), & \text{if } \boldsymbol{\mathcal{F}}_n = \{\mathbf{l}_n, \boldsymbol{\alpha}_n\}, \quad (28b) \end{cases}$$

respectively.

In (27-b), the birth density $b_{n|n-1}(\{\mathbf{l}_n, \boldsymbol{\alpha}_n\})$ specifies the initial distribution of a singleton state $\{\mathbf{l}_n, \boldsymbol{\alpha}_n\}$ after the PU is re-emitted or re-appeared, i.e.,

$$b_{n|n-1}(\{\mathbf{l}_n, \boldsymbol{\alpha}_n\}) \triangleq p_{n|n-1}\left(\{\mathbf{l}_n, \boldsymbol{\alpha}_n\}|q_n = 1, q_{n-1} = 0\right),$$

which will be discussed in subsequent *Section III.E.4*. Another prior transitional probability in (28-b) is:

$$\varpi_{n|n-1}(\{\mathbf{l}_n, \boldsymbol{\alpha}_n\}|\{\mathbf{l}_{n-1}, \boldsymbol{\alpha}_{n-1}\}) = \varpi_{n|n-1}(\mathbf{l}_n|\mathbf{l}_{n-1}) \times \varpi_{n|n-1}(\boldsymbol{\alpha}_n|\boldsymbol{\alpha}_{n-1}). \quad (29)$$

Recall the previous (15)–(17), the transitional density of PU's mobile positions will be specified by:

$$\varpi_{n|n-1}(\mathbf{l}_n|\mathbf{l}_{n-1}) = \frac{1}{\sqrt{2\pi}\sigma_v} \times \exp\left(-\frac{||\mathbf{l}_n - \mathbf{l}_{n-1}||^2}{2\sigma_v^2}\right) \times \frac{1}{\sqrt{2\pi}\sigma_\theta} \times \exp\left(-\frac{|\mathtt{ang}(\mathbf{l}_n) - \mathtt{ang}(\mathbf{l}_{n-1})|}{2\sigma_\theta^2}\right), \quad (30)$$

where $\mathtt{ang}(\cdot)$ gives the angle of a displacement vector. The other prior transitional density in (29) is given by:

$$\varpi_{n|n-1}(\boldsymbol{\alpha}_n|\boldsymbol{\alpha}_{n-1}) = \prod_{r=1}^{R} \rho_{k_1(n,r)\to k_2(n,r)},$$

where $k_1(n, r) \in \{0, 1, 2, \ldots, K-1\}$ and $k_2(n, r) \in \{0, 1, 2, \ldots, K-1\}$ denotes two indexes of the rth PU-SU link at time n under a constraint $|k_1(n, r) - k_2(n, r)| \leq 1$.

4) Estimations of RFS: It is seen from (26) that the FISST PDF $p_{n|n}(\boldsymbol{\mathcal{F}}_n|\mathbf{z}_{1:n})$ depends primarily on two terms, i.e., the posterior density of PU's existence (i.e., $q_{n|n}$) and the *a posteriori* spatial PDF of hidden link states $\{\mathbf{l}_n, \boldsymbol{\alpha}_n\}$. Here, the posterior density of PU's existence is:

$$q_{n|n} = \Pr\left(|\boldsymbol{\mathcal{F}}_n| = 1|\mathbf{z}_{1:n}\right), \quad (31)$$

and the other posterior spatial PDF of $\boldsymbol{\mathcal{F}}_n = \{\mathbf{l}_n, \boldsymbol{\alpha}_n\}$ is:

$$p_{n|n}\left(\boldsymbol{\mathcal{F}}_n = \{\mathbf{l}_n, \boldsymbol{\alpha}_n\}\right) = \Pr\left(\{\mathbf{l}_n, \boldsymbol{\alpha}_n\}|\mathbf{z}_{1:n}\right). \quad (32)$$

C. Bernoulli Filtering for BRFS

Relying on the formulated DSM and measurements $\mathbf{z}_{1:n}$, the posterior densities of RFS will be estimated recursively. Given *a priori* transitional densities in (29)–(30) and the likelihood densities of (19)–(20), a generalized two-stage recursive scheme will be applied to derive the posterior distribution of $\boldsymbol{\mathcal{F}}_n$, i.e.,

$$p_{n|n-1}(\boldsymbol{\mathcal{F}}_n|\mathbf{z}_{1:n-1}) = \int_{\boldsymbol{\mathcal{F}}_{n-1}} \phi_{n|n-1}(\boldsymbol{\mathcal{F}}_n|\boldsymbol{\mathcal{F}}_{n-1}) p_{n-1|n-1}(\boldsymbol{\mathcal{F}}_{n-1}|\mathbf{z}_{1:n-1})\delta\boldsymbol{\mathcal{F}}_{n-1}, \quad (33)$$

$$p_{n|n}(\boldsymbol{\mathcal{F}}_n|\mathbf{z}_{1:n}) = \frac{\varphi_n(\mathbf{z}_n|\boldsymbol{\mathcal{F}}_n) p_{n|n-1}(\boldsymbol{\mathcal{F}}_n|\mathbf{z}_{1:n-1})}{\int_{\boldsymbol{\mathcal{F}}_n} \varphi_n(\mathbf{z}_n|\boldsymbol{\mathcal{F}}_n) p_{n|n-1}(\boldsymbol{\mathcal{F}}_n|\mathbf{z}_{1:n-1})\delta\boldsymbol{\mathcal{F}}_n}. \quad (34)$$

A major difference between the above generalized estimation of RFS and traditional Bayesian inference in (23)–(24) is that, rather than the distribution integration, here a set integration (i.e., $\delta\boldsymbol{\mathcal{F}}_n$) will be taken [32]–[34].

1) Prediction Stage: During the 1st stage, two predict densities, i.e., $q_{n|n-1}$ and $p_{n|n-1}(\{\mathbf{l}_{n-1}, \boldsymbol{\alpha}_{n-1}\})$, are derived. One may refer to [32], [33] for details.

Remark 1: The predicted existence density and spatial density will be propagated via:

$$q_{n|n-1} = p_b \times (1 - q_{n-1|n-1}) + p_s \times q_{n-1|n-1}, \quad (35)$$

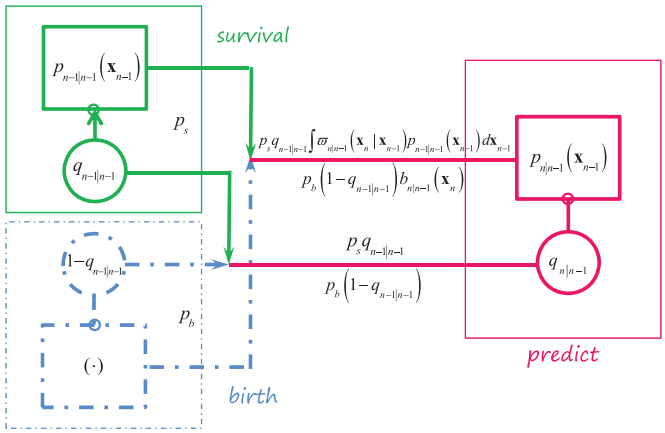

Fig. 2. An illustration of predicting procedure. For clarity, here $\mathbf{x}_n = \{\mathbf{l}_n, \boldsymbol{\alpha}_n\}$.

and (36), shown at the bottom of the page, respectively.

It is noteworthy that, from (35) and (36), both the predicted existence density $q_{n|n-1}$ and the spatial density $p_{n|n-1}(\{\mathbf{l}_n, \boldsymbol{\alpha}_n\})$ will contain two complementary terms, i.e., the *birth* component and the *survival* component. A logical evolution structure of these two predicted densities is illustrated by Fig. 2.

2) Update Stage: During the 2nd stage, the above two predicted densities will be updated based on the new observation $\mathbf{z}_n$, see [32], [33].

Remark 2: The existence density $q_{n|n}$ and the spatial density $p_{n|n}(\{\mathbf{l}_n, \boldsymbol{\alpha}_n\})$ are updated [see (37)-(38) at the bottom of the page, respectively]. Here, the term $r_n(\mathbf{z}_n|\{\mathbf{l}_n, \boldsymbol{\alpha}_n\})$ accounts for a ratio between the likelihoods of two hypothesis, i.e.,

$$r_n\left(\mathbf{z}_n|\{\mathbf{l}_n, \boldsymbol{\alpha}_n\}\right) \triangleq \varphi_n\left(\mathbf{z}_n|\{\mathbf{l}_n, \boldsymbol{\alpha}_n\}\right)/\varphi_n(\mathbf{z}_n|\varnothing).$$

Based on the generalized Bayesian inference, the estimation of two posterior densities, i.e., the existence probability $q_{n|n}$ and the spatial PDF $p_{n|n}(\{\mathbf{l}_n, \boldsymbol{\alpha}_n\})$, will be obtained.

D. Refinement Mechanisms

Considering the slowly-varying fading channel $\boldsymbol{\alpha}_n$ remain quasi-static in L successive slots, we further suggest two improving mechanisms to maximize the functioning of the recursive estimation scheme.

1) The first mechanism is referred to ***observation accumulation***. As the fading state $\boldsymbol{\alpha}_n$ will be unchanged in a short period, after its transition has occurred at a switching time $n' = \lfloor n/L \rfloor$, the innovation observations of the subsequent L slots will be used to promote the estimation accuracy of $\boldsymbol{\alpha}_n$. That is, in the time slot $n = Ln' + l (0 < l < L)$, part of previous observations (i.e., in the case of $\hat{s}_n = 1$) will be cumulated, and a new observation is re-defined as:

$$z_{n'L+l,r} = z_{n'L,r} + \sum_{t=1}^{l_1} z_{n'L+t,r}. \tag{39}$$

Here, $l_1 \leq l$ accounts for the number of occurrences of PU's active state (i.e., H_1) in the previous l slots, i.e., $n'L, \ldots, n'L+l$. As the summation of independent Gaussian variables (i.e., $z_{n'L+t,r}$) is also Gaussian distributed, the accumulated observation $z_{n'L+l,r}$ will also follow the Gaussian distributions, i.e.,

$$\varphi(z_{n'L+l,r}|s_n = 0) \sim \mathcal{N}(l_1 M\sigma_w^2, 4l_1 M\sigma_w^4), \tag{40}$$

$$\begin{aligned}\varphi(z_{n'L+l,r}|\alpha_{n,r}, d_{n,r}, s_n = 1) \\ \sim \mathcal{N}\left\{M\sum_{t=1}^{l_1}\left(\frac{E_s\alpha_{n,r}^2}{d^{\epsilon}_{n'L+t,r}} + \sigma_w^2\right),\right. \\ \left. M\sum_{t=1}^{l_1}\left(\frac{\sigma_w^2 E_s\alpha_{n,r}^2}{d^{\epsilon}_{n'L+t,r}} + 4\sigma_w^4\right)\right\}.\end{aligned} \tag{41}$$

Note that, the accumulated observation and its likelihood are applied only to refine $\boldsymbol{\alpha}_n$ and s_n, after deriving the PU's position $\mathbf{l}_n$ and the rough estimations of $\boldsymbol{\alpha}_n$ and s_n premised on the current observation $\mathbf{z}_n$. The underlying principle of the accumulation mechanism is that, with more likelihood information exploited, the estimation of fading gains $\boldsymbol{\alpha}_n$ accompanying unknown PU states will be reinforced.

2) The second mechanism is referred to ***homologous estimation***. The main motivation is that the predicting/updating procedure should be implemented in accordance with the *quasi-static* transitions of the fading states with a static length L. Different from the inference of classical RFS [32], [34], in the suggested scheme now the predicting and updating procedures utilize the previous densities $p_{n'L-1|n'L-1}(\boldsymbol{\alpha}_{n'L-1})$ and $p_{n|Ln'-1}(\boldsymbol{\alpha}_n)$, respectively.

Conditioned on the accumulated observation in (39), it is supposed that the spatial distribution of the $(Ln'-1)$th time has probably become very accurate, after combining the former

$$\begin{aligned}p_{n|n-1}(\mathbf{l}_n, \boldsymbol{\alpha}_n) = &\frac{p_b(1-q_{n-1|n-1})b_{n|n-1}(\mathbf{l}_n, \boldsymbol{\alpha}_n)}{q_{n|n-1}} \\ &+ \frac{p_s q_{n-1|n-1}\int \varpi_{n|n-1}(\mathbf{l}_n, \boldsymbol{\alpha}_n|\mathbf{l}_{n-1}, \boldsymbol{\alpha}_{n-1})p_{n-1|n-1}(\mathbf{l}_{n-1}, \boldsymbol{\alpha}_{n-1})d\mathbf{l}_{n-1}d\boldsymbol{\alpha}_{n-1}}{q_{n|n-1}}.\end{aligned} \tag{36}$$

$$q_{n|n} = \frac{q_{n|n-1}\int_{\mathbf{l}_n\in\mathbb{R}^2, \boldsymbol{\alpha}_a\in\mathcal{A}^R} r_n(\mathbf{z}_n|\mathbf{l}_n, \boldsymbol{\alpha}_n)p_{n|n-1}(\{\mathbf{l}_n, \boldsymbol{\alpha}_n\})d\mathbf{l}_n d\boldsymbol{\alpha}_n}{(1-q_{n|n-1}) + q_{n|n-1}\int r_n(\mathbf{z}_n|\mathbf{l}_n, \boldsymbol{\alpha}_n)p_{n|n-1}(\{\mathbf{l}_n, \boldsymbol{\alpha}_n\})d\mathbf{l}_n d\boldsymbol{\alpha}_n}, \tag{37}$$

and

$$p_{n|n}(\{\mathbf{l}_n, \boldsymbol{\alpha}_n\}) = \frac{r_n(\mathbf{z}_n|\{\mathbf{l}_n, \boldsymbol{\alpha}_n\})p_{n|n-1}(\{\mathbf{l}_n, \boldsymbol{\alpha}_n\})}{\int r_n(\mathbf{z}_n|\{\mathbf{l}_n, \boldsymbol{\alpha}_n\})p_{n|n-1}(\{\mathbf{l}_n, \boldsymbol{\alpha}_n\})d\mathbf{l}_n d\boldsymbol{\alpha}_n}. \tag{38}$$

$1 < l_1 < L$ historical observations. The predicting of fading states in (36), therefore, will rely on the spatial density of time $L(n'-1)+L-1 = Ln'-1$ other than the previous time $(n-1)$, see (42) at the bottom of the page. Here, the prior density can be further simplified to $\varpi_{n|n-1}(\{\mathbf{l}_n, \boldsymbol{\alpha}_n\}|\{\mathbf{l}_{n-1}, \boldsymbol{\alpha}_{n'l-1}\}) = \varpi_{n|n-1}(\mathbf{l}_n|\mathbf{l}_{n-1}) \times \varpi_{n|nL'-1}(\boldsymbol{\alpha}_n|\boldsymbol{\alpha}_{n'L-1})$.

E. PF-Based Implementation

Noted from (36) that the derivation of a predicted spatial density $p_{n|n-1}(\{\mathbf{l}_n, \boldsymbol{\alpha}_n\})$ relies on the marginalization of continuous distributions. As far as the integration on the $(2+R)$-dimensional density is concerned, the implementation will be computationally intractable. To cope with the difficulty, a numerical approach, i.e., the SIS based PF, is suggested to alleviate the complexity of Bayesian inference.

1) PF: In essence, PF belongs to a simulated numerical method, which approximates the complex distribution via a group of random discrete measures (i.e., particles) $\mathbf{x}_n^{(i)}$ with the evolving probability masses (or weights) $w_n^{(i)} (i = 1, 2, \ldots, I)$ [35], i.e., $p_n(\mathbf{x}) \backsimeq \sum_{i=0}^{I} \delta\left(\mathbf{x} - \mathbf{x}_n^{(i)}\right) \times w_n^{(i)}$. Usually, PF consists of two steps. Firstly, a proposal density $\xi_n\left(\mathbf{x}_n^{(i)}|\mathbf{x}_{1:n-1}^{(i)}, z_{1:n-1}\right)$ that is related with the target density $p_n(\mathbf{x})$ is designed, from which total I simulated particles are drawn, i.e., $\xi_n\left(\mathbf{x}_n^{(i)}|\mathbf{x}_{1:n-1}^{(i)}, z_{1:n-1}\right)$. Secondly, the associated importance weights $w_n^{(i)}$ are updated via:

$$w_n^{(i)} = w_{n-1}^{(i)} \times \frac{\varphi_n\left(\mathbf{z}_n \left| \mathbf{x}_n^{(i)} \right.\right) \times \varpi_{n|n-1}\left(\mathbf{x}_n^{(i)} \left| \mathbf{x}_{n-1}^{(i)} \right.\right)}{\xi_n\left(\mathbf{x}_n \left| \mathbf{x}_{1:n-1}^{(i)}, \mathbf{z}_{1:n-1} \right.\right)}. \quad (43)$$

In practice, a *re-sample* procedure will be adopted in order to eliminate particles with negligible weights [35].

2) Bernoulli PF: For the DS application, the PF is used to approximate the predicted spatial density $p_{n|n-1}(\mathbf{x})$, i.e.,

$$\hat{p}_{n|n-1}(\mathbf{x}) \backsimeq \sum_{i=1}^{I} w_{n|n-1}^{(i)} \delta\left(\mathbf{x} - \mathbf{x}_{n|n-1}^{(i)}\right). \quad (44)$$

For clarity, here $\mathbf{x}_{n|n-1} \triangleq \{\mathbf{x}\mathbf{l}_{n|n-1}, \mathbf{x}\boldsymbol{\alpha}_{n|n-1}\}$ denotes the mixture hidden particles. As seen from (36), $p_{n|n-1}(\mathbf{x})$ is composed of two parts, i.e., a survival component and the other birth component. A proposal distribution of two pieces is thereby designed to simulate to the mixture particles $\left(\mathbf{x}_{n|n-1}^{(i)}, w_{n|n-1}^{(i)}\right)$, i.e.,

$$\mathbf{x}_{n|n-1}^{(i)} \sim \begin{cases} \beta_n\left(\mathbf{x}_{n|n-1}|\mathbf{z}_{1:n-1}\right), & (45a) \\ \qquad i = 1, 2, \ldots, B, & \\ \xi_n\left(\mathbf{x}_{n|n-1} \left| \mathbf{x}_{n-1|n-1}^{(i)}, \mathbf{z}_{1:n-1} \right.\right), & (45b) \\ \qquad i = B+1, \ldots, I. & \end{cases}$$

If collating (45) with (36), the first birth term is approximated by B particles, while the second survival term is simulated via the later $(I - B)$ particles. Given total I simulated measures $\mathbf{x}_{n|n-1}^{(i)}$, the weights are updated by [32]:

$$w_{n|n-1}^{(i)} \sim \begin{cases} \frac{p_b(1-q_{n|n})}{q_{n|n-1}} \times \frac{b_{n|n-1}\left(\mathbf{x}_{n|n-1}^{(i)}\right)}{\beta_n\left(\mathbf{x}_{n|n-1}^{(i)}|\mathbf{z}_{1:n-1}\right)} \times \frac{1}{B}, & \\ \qquad i = 1, 2, \ldots, B, & (46a) \\ \frac{p_s q_{n-1|n-1}}{q_{n|n-1}} \cdot \frac{\varpi_{n|n-1}\left(\mathbf{x}_{n|n-1}^{(i)}|\mathbf{x}_{n-1|n-1}^{(i)}\right)}{\xi_n\left(\mathbf{x}_{n|n-1}|\mathbf{z}_{1:n-1}\right)} w_{n-1|n-1}^{(i)}, & \\ \qquad i = B+1, \ldots, I. & (46b) \end{cases}$$

Once the proposal birth density $\beta_n\left(\xi_n\left(\mathbf{x}_{n|n-1}|\mathbf{x}_{1:n-1}^{(i)}, z_{1:n-1}\right)\right)$ and the other proposal survival density $\xi_n\left(\mathbf{x}_{n|n-1} \left| \mathbf{x}_{n-1|n-1}^{(i)}, \mathbf{z}_{1:n-1} \right.\right)$ are specified properly, then the Bayesian inference will be realized, and $p_{n|n-1}(\mathbf{x})$ can be numerically evaluated.

3) Proposal Survival-Density: In practice, the proposal survival density is simple to obtain. First, with $(I - B)$ predicted particle and their weights $\left\{\mathbf{x}_{n-1|n-2}^{(i)}, w_{n-1|n-2}^{(i)}\right\}$, the posterior density of time $(n-1)$ will be estimated and the corresponding particle weights are updated via:

$$w_{n-1|n-1}^{(i)} \propto \varphi_n\left(\mathbf{z}_{n-1} \left| \boldsymbol{\mathcal{F}}_{n-1|n-2}^{(i)} \right.\right) \times w_{n-1|n-2}^{(i)}. \quad (47)$$

Second, $(I - B)$ discrete particles are drawn from $\hat{p}_{n-1|n-1}(\mathbf{x}) = \sum_{i=0}^{I} w_{n-1|n-1}^{(i)} \times \delta\left(\mathbf{x} - \mathbf{x}_{n-1|n-1}^{(i)}\right)$. The $(I - B)$ new particles are survival and further reserved for the subsequent time n [32].

4) Proposal Birth-Density: As far as two independent link states $\mathbf{l}_n$ and $\boldsymbol{\alpha}_n$ are concerned, a compound proposal birth density should be designed, i.e.,

$$\begin{aligned} \beta_n\left(\mathbf{x}_{n|n-1}|\mathbf{z}_{1:n-1}\right) &= b_{n|n-1}(\{\mathbf{l}_n, \boldsymbol{\alpha}_n\}) \\ &= b_{n|n-1}(\mathbf{l}_n) \times b_{n|n-1}(\boldsymbol{\alpha}_n). \end{aligned} \quad (48)$$

(**a**) For the sub-density of birth particles corresponding to the time-varying fading state, i.e., $b_{n|n-1}(\mathbf{x}\boldsymbol{\alpha}_n)$, we suggest an adaptive birth density, which is determined jointly by the prior transitional density $\varpi_{n|n-1}(\boldsymbol{\alpha}_n|\boldsymbol{\alpha}_{n-1})$ and the accumulated measurement $\mathbf{z}_{n'L-1}$. Further combining the homologous estimation of fading channels, it is specified as:

$$\begin{aligned} b_{n|n-1}(\boldsymbol{\alpha}_n) \triangleq \int & \varpi_{n|n'L-1}(\boldsymbol{\alpha}_n|\vec{\boldsymbol{\alpha}}_{n'L-1}) \\ & \times b_{n'L-1}(\vec{\boldsymbol{\alpha}}_{n'L-1}|\mathbf{z}_{n'L-1}) d\vec{\boldsymbol{\alpha}}_{n'L-1}, \end{aligned} \quad (49)$$

where the intermediate birth density $b_{n'L-1}(\vec{\boldsymbol{\alpha}}_{n'L-1}|\mathbf{z}_{n'L-1})$ is given by $\prod_{r=1}^{R} b_{n'L-1}(\vec{\alpha}_{n'L-1,r}|z_{n'L-1,r})$. In the considera-

$$\begin{aligned} & p_{n|n-1}(\{\mathbf{l}_n, \boldsymbol{\alpha}_n\}|\mathbf{z}_{1:n-1}) \\ &= \frac{p_b(1-q_{n-1|n-1}) b_{n|n-1}(\{\mathbf{l}_n, \boldsymbol{\alpha}_n\})}{q_{n|n-1}} \\ &\quad + \frac{p_s q_{n-1|n-1} \int \varpi_{n|n-1}(\{\mathbf{l}_n, \boldsymbol{\alpha}_n\}|\{\mathbf{l}_{n-1}, \boldsymbol{\alpha}_{n'L-1}\}) p_{n-1|n-1}(\{\mathbf{l}_{n-1}, \boldsymbol{\alpha}_{n'L-1}\}) d\mathbf{l}_{n-1} d\boldsymbol{\alpha}_{n'L-1}}{q_{n|n-1}}. \end{aligned} \quad (42)$$

tion of the 1st-order DSFC model, the posterior component in (49) are given by:

$$b_{n'L-1}(\vec{\alpha}_{n'L-1,r} = \mathrm{A}_j | z_{n'L-1,r}) = \begin{cases} \frac{1}{3}, & \text{if } \hat{\alpha}_{n'L-1,r} | z_{n'L-1,r} \to \mathrm{A}_i, |i-j| \le 1, \quad (50a) \\ 0, & \text{if } \hat{\alpha}_{n'L-1,r} | z_{n'L-1,r} \to \mathrm{A}_i, |i-j| > 1. \quad (50b) \end{cases}$$

Note that, here the intermediate state $\vec{\boldsymbol{\alpha}}_{n'L-1}$ is generated to increase the diversity of birthed particles $\boldsymbol{\alpha}_n$, which, to some extent, may avoid the local solution aroused by the erroneous estimations $\{\hat{\alpha}_{n'L-1,r}\}_{r=1}^{R}$.

(**b**) For the other birth sub-density, i.e., $b_{n|n-1}(\mathbf{xl}_n)$, the major challenge is how to address the aforementioned likelihood dispersion problem aroused by the sudden cease of PU's emission (i.e., $s_n = 0$). If this happens, there is no likelihood information can be utilized. To tackle the difficult problem, we design a flexible sub-density by integrating a promising AHE mechanism. The principle is that, when the PU jumped into the silent state at time $n-J$, its positions of subsequent times will be predicted, premised on the previously estimated speed and orientation. At the same time, the uncertainty introduced by the predicted positions will be updated when simulating new birth particles (corresponding to $\mathbf{xl}$) once this PU re-emits.

For clarity, the lasting length of $s_{n-1} = 0$ is denoted by J, i.e., $s_{n-1-\tau} = 0$ for $0 < \tau < J$ and $s_{n-1-J} = 1$. To sum up, the AHE involves essentially two stages, i.e., the position predicting and the uncertainty updating.

1) If the PU enters to H_0 at time $(n-J)$, then in subsequent time $n_\tau = n - J + \tau (0 < \tau < J)$, its unknown positions will be predicted based on the previously estimated speed $\hat{v}_{n-J}$ and moving orientation $\hat{\theta}_{n-J}$ [20], as well as the tracked position of time $(n-J)$, i.e.,

$$\hat{\mathbf{l}}_{n-J+\tau} = [\hat{x}_{n-J} \ \hat{y}_{n-J}]^T + \tau \hat{v}_{n-J} \times [\cos(\hat{\theta}_{n-J}) \ \sin(\hat{\theta}_{n-J})]^T. \quad (51)$$

In practice, $\hat{v}_{n-J}$ and $\hat{\theta}_{n-J}$ will be derived from the trajectory of previously tracked positions, i.e., $\{\mathbf{l}_{n-J-L}, \ldots, \mathbf{l}_{n-J}\}$. Note from (51) that the estimated velocity will be of great significance to AHE. Thus, an autoregressive (AR) model is suggested to suppress the estimation bias of $\hat{v}_{n-J}$ and $\hat{\theta}_{n-J}$, i.e.,

$$\hat{v}_{n-J} = \sum_{\iota=1}^{L_b} \varepsilon^{L_b-\iota} \times ||\hat{\mathbf{l}}_{n-J-\iota} - \hat{\mathbf{l}}_{n-J-\iota-1}||_2^2, \quad (52)$$

$$\hat{\theta}_{n-J} = \sum_{\iota=1}^{L_b} \varepsilon^{L_b-\iota} \times \mathtt{ang}(\hat{\mathbf{l}}_{n-J-\iota} - \hat{\mathbf{l}}_{n-J-\iota-1}). \quad (53)$$

Here, ε denotes a weighting parameter, which may be set empirically to $0.5 \sim 0.8$; $L_b \in [1, 10]$ denotes a backtracking length.

2) Assume the PU re-emits at the time n after residing in the silence state for successive J slots. Thus, the PU's position should be re-birthed within an enlarged range, by fully utilizing the *a priori* information of the mobility model. To do so, a birth sub-density is specified as:

$$b_{n|n-1}(\mathbf{x}) = f_v(v_n|\eta J) \times f_\theta(\theta_n|J), \quad (54)$$

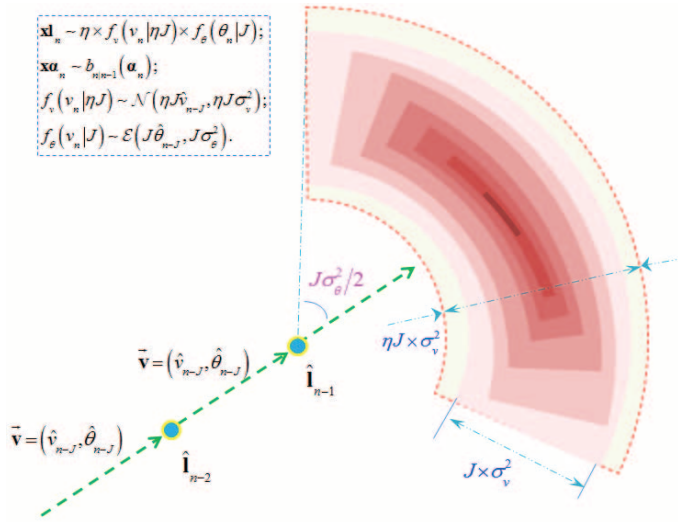

Fig. 3. The birth process of two associative states. After total J-step predictions under $s_{n-J:n-1} = 0$, the birth uncertainty of PU's positions will be determined by a 2-D sector region. Here, $\mathbf{xl}_n$ accounts for possible PU's positions after J silence slots, while $\mathbf{x}\boldsymbol{\alpha}_n$ is the associated fading states.

where the speed density $f_v(v_n|\eta J)$ and the orientation density $f_\theta(\theta_n|J)$ jointly designate a 2-dimension space.

$$f_v(v_n|\eta J) \sim \mathcal{N}(\eta J \hat{v}_{n-J}, \eta J \sigma_v^2), \quad (55)$$

$$f_\theta(\theta_n|J) \sim \mathcal{E}(\hat{\theta}_{n-J}, J\sigma_\theta^2). \quad (56)$$

Here, $\eta > 1$ accounts for the *allowance factor* which is employed to address the additional uncertainty (or error) of the estimated fading states $\boldsymbol{\alpha}_{n-1}$, which in practice can be determined by:

$$\eta = \sqrt{\max(1/\mathrm{A}_{k_2}^2 - 1/\mathrm{A}_{k_1}^2)}, 1 \le k_1, k_2 \le K. \quad (57)$$

It is expected from (54)–(56) that, with the increase of J, the horizon (or cover area) of the birth sub-density $b_{n|n-1}(\mathbf{x})$ will be expanded accordingly, as illustrated by Fig. 3. Thus, the PU's mobile positions would be tracked by the above uncertainty adaption strategy, even after a long suspending of PU's emission. Notice that, in the following emission slots $n+J$, the uncertainty of the birth sub-density will be reset to 1 in the case of $s_{n+J} = 1$.

With the designed survival-density and birth-density, total I discrete particles can be drawn from a unified proposal distribution, i.e., $\mathbf{x}_{n-1|n-1}^{(i)} \sim \xi_n\left(\mathbf{x}_{n|n-1}|\mathbf{x}_{n-1|n-1}^{(i)}, \mathbf{z}_{1:n-1}\right)$, for $i = 1, \ldots, B, B+1, \ldots, I$ [32]. Then, the importance weights of new particles will be updated via (46).

5) Simplified Implementations: In order to cover the 2-dimensional continuous mobile region and another R-dimensional discrete states-space, the required number of particles will be considerably huge. In practice, we adopt a simplified implementation scheme. To be specific, each position particle (i.e., $\mathbf{xl}_n$) carries only one possible fading state, i.e., the 1st-order prior transitions from $\hat{\boldsymbol{\alpha}}_{n-1}$. Then, B position particles (i.e., $\mathbf{xl}_n$) are drawn from the sub-birth density of $b_{n|n-1}(\mathbf{l}_n)$, and finally, the predicted particle $\mathbf{x}\boldsymbol{\alpha}_n$ will be appended to construct the mixture particles $\mathbf{x}_n$.

As the proposal birth density is premised on the prior transitions, the weights of birthed particles will be updated by:

$$w_{n|n-1}^{(i)} \propto \frac{p_b(1-q_{n-1|n-1})}{q_{n|n}} \times \frac{1}{B}, \quad i=1,\ldots,I. \tag{58}$$

Thus, the predicted spatial density $p_{n|n-1}(\{\mathbf{l}_n, \boldsymbol{\alpha}_n\})$ will be derived approximately, with the marginalization replaced by the summation by using $\left(\mathbf{x}_{n|n-1}^{(i)}, w_{n|n-1}^{(i)}\right)$.

Moving on, we can obtain $\hat{q}_{n|n}$ and estimate PU's state via:

$$\hat{s}_n = \begin{cases} 1, & \text{if } \hat{q}_{n|n} \geq \gamma, \quad (59a) \\ 0, & \text{if } \hat{q}_{n|n} < \gamma, \quad (59b) \end{cases}$$

where γ is configured to 0.5 under a Bayesian criterion. Similarly, the PU's positions and fading states will be estimated by maximizing the approximated spatial density, i.e.,

$$(\hat{\mathbf{l}}_n, \hat{\boldsymbol{\alpha}}_n) = \arg \max_{\mathbf{l}_n \in \mathbb{R}^2, \boldsymbol{\alpha}_n \in \mathcal{A}^R} \hat{p}_{n|n}\left(\{\mathbf{l}_n, \boldsymbol{\alpha}_n\}\right). \tag{60}$$

6) Algorithm Flow: A schematic structure of the proposed algorithm is plotted in Fig. 4. First, two predicted densities $q_{n|n-1}$ and $p_{n|n-1}(\mathbf{x})$ will be estimated. Then, they will be updated by utilizing the new observation $\mathbf{z}_n$. Finally, in the case of $q_{n|n} < \gamma$ and $J > 1$, the designed AHE will be applied. In order to realize AHE, a counter J is employed, which is of practical use to update the uncertainty of the birth uncertainty.

7) Complexity: The algorithm complexity is roughly measured by the total number of multiplications. First, in order to obtain RSS observations, $O(RM)$ multiplications are required. Second, the number of multiplications required by the Bayesian estimation is proportional to the size of simulated particles (i.e., I) in PF. Here, the computation of each related likelihood densities is basically measured by ϑ, where ϑ is related with the representative precision of numbers and various adopted algorithms [36]. To sum up, the total complexity of the new algorithm will be given by $O(RM + I\vartheta)$.

IV. Numerical Simulations

In the following simulations, the performance of the new DS scheme will be evaluated. Three performance metrics, i.e., the sensing accuracy of PU's status, the localization errors and the channel estimation errors, will be studied numerically.

1) Sensing Metric: As a Bayesian approach, unlike the classical NP criterion [7], [8], a total correct probability is used as the sensing performance metric, as in [12], [13], [37].

$$P_D \triangleq 1 - P(H_1)P_m - P(H_0)P_f, \tag{61}$$

where the false alarm P_f confines the utilization of vacant spectrum, while a missed detection probability P_m controls the interferences caused to PU. Note that, the new *compound* metric remains quite different from that of a classical NP criterion, in which the objective is either to minimize P_m for a target P_f, or to minimize the P_f for a target P_m.

In following analysis, rather than focusing on a single P_d by prescribing P_f, we will evaluate the total correct probability P_D. It is suggested that, with the new metric, the spectral utilization of unused PU's spectrum and the potential interference to PU will be jointly considered [20], [37], [38]. Note that, unlike an NP criterion, now the P_f *cannot* be fixed under an MAP criterion. To be specific, when imposing a threshold to fix P_f as in classical ED, the estimations of fading channels and PU's locations would not be utilized. The new metric P_D, therefore, is more suitable to evaluate the designed Bayesian scheme. It is demonstrated that, by exploiting the informative hidden states and an MAP criterion, in the proposed Bayesian approach an improved P_D will also result in the promotion of both P_d and P_f compared to an NP criterion [13].

2) Localization Metric: For the localization of a mobile PU, as a commonly used metric, the root mean square error (RMSE) of estimated locations is investigated, i.e.,

$$\text{MSE} \triangleq \mathsf{E}\left\{\sqrt{\frac{1}{N} \times \sum_{n=1}^{N} ||\mathbf{l}_n - \hat{\mathbf{l}}_n||_2^2}\right\}. \tag{62}$$

3) Channel Estimation Metric: When it comes to the estimation of time-correlated fading channels, a similar MSE performance will be used, i.e.,

$$\text{RMSE} \triangleq \mathsf{E}\left\{\frac{1}{R} \times \sum_{r=1}^{R} \sqrt{\frac{1}{N} \sum_{n=1}^{N} ||\boldsymbol{\alpha}_{n,r} - \hat{\boldsymbol{\alpha}}_{n,r}||_2^2}\right\}. \tag{63}$$

A. Simulation Configurations

In the simulations, $R = 4$ SUs are deployed on the vertexes of a square (maybe an indoor office or an outdoor square, etc.), while the PU is moving randomly within the grid region with a side length of 100 m. The prior locations of 4 SU nodes are (0, 0), (0, 100), (100, 0), (100, 100). Without losing generality, in the assumed GMM model the initial speed is $v_0 = 0.005$ m/slot and the initial orientation is $\theta_0 = 0.785$ rad (i.e., 45°c), which may correspond to a mobile human carrying the PU device. The variance of PU's speed is $\sigma_v^2 = 0.0002$ and the variance of PU's orientation is $\sigma_\theta^2 = 0.02$. Based on multiple random trajectories, the average signal-to-noise ratio (SNR) will be statistically evaluated, given the Gaussian noise variance σ_w^2. For the considered DSMC, the variance of Rayleigh distribution may be basically insignificant to the performance analysis, which is set to $\sigma_\alpha^2 = 0.1$; the number of discrete representative states is $K = 8$. The transitional probability of PU states is set to $(p_b, p_s) = (0.8, 0.8)$.

B. Different Static Length L

In the first experiment, the effect of different fading rates (or the static length L) is investigated. The size of discrete particles are $I = 500$ and the number of birth particles are $B = 250$. Total 80 trajectories have been simulated and, in each independent realization, 5000 sensing-transmission slots are evaluated with a new generated fading channel.

In Fig. 5, the localization RMSE of the mobile PU is plotted. As we have indicated before, the static length ranges from 10 to 60. So, in the analysis two realistic static lengths are studied, i.e., $L = 20$ and $L = 50$. For convenience, assume the static length L is normalized by T_F, thus f_d will be approximately proportional to $1/L$. The sample size is $M = 100$. It is seen from numerical results that, given the high SNRs, the PU's mobile locations will be tracked accurately even its emission is shut off intermittently. When the SNR is configured to 15 dB, the RMSE may approach 1.32 m with a static length of $L = 50$. Meanwhile, it is also noted that the localization RMSE, given

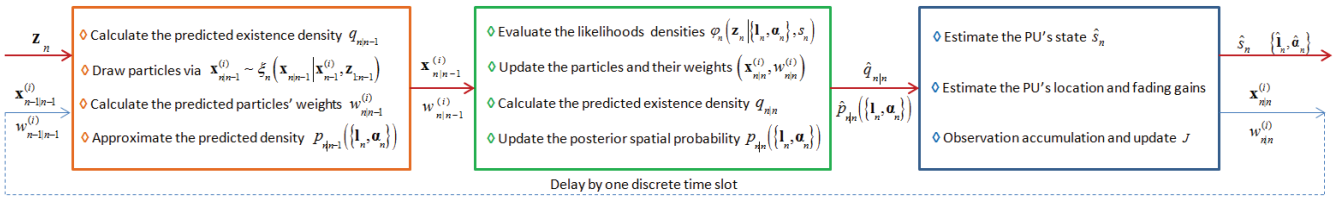

Fig. 4. Schematic flow of the suggested Algorithm.

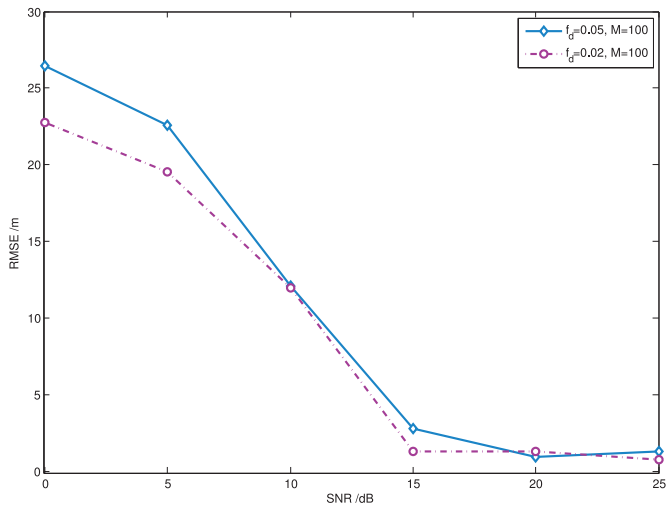

Fig. 5. Localization RMSE of the PU under different static length L.

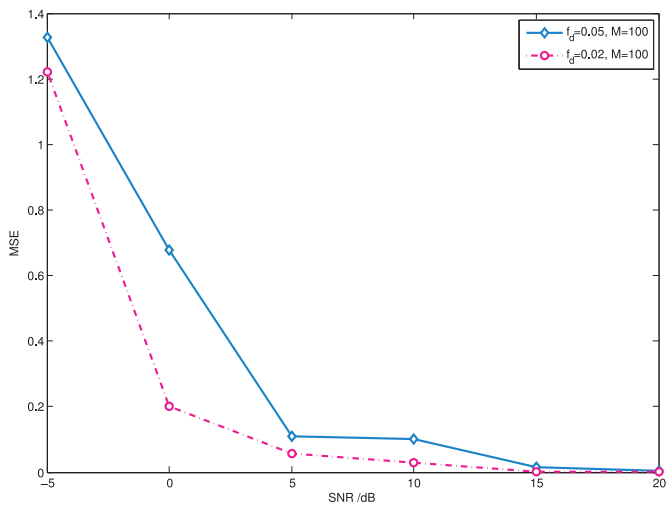

Fig. 6. Channel estimation MSE of the PU-SU link under different static length L.

the discontinuity of PU's emissions and time-varying fading channels, will be basically converged under two static lengths $(L = 20, 50)$ when SNR $>$ 15 dB. Also, we find the RMSE of $L = 50$ will be slightly superior to that of $L = 20$. This is mainly because, with the observation accumulation mechanism, the more profound refinement on channel estimations will be achieved by a larger L.

A similar trend in Fig. 6 further verifies the above analysis, in which the channel estimation MSE of $L = 50$ is much smaller than that of $L = 20$. For example, if SNR is configured to 10 dB, the numerically derived MSE is about 0.027 for a static length of $L = 50$, while it will be increased to 0.1 given a faster fading channel of $L = 20$.

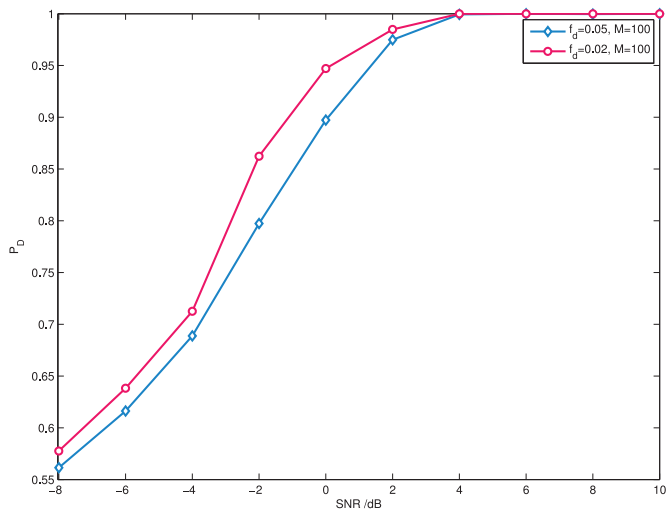

Fig. 7. Total correct probability P_D under different static length L.

The total correct probability P_D is shown by Fig. 7. We note that, for both $L = 20$ and $L = 50$, the total correct probability P_D will approach 1 when the SNR surpasses 4 dB and the sample size is $M = 100$. It is also observed that the total correct probability P_D of $L = 50$ will be superior to that of $L = 20$. Combined with Figs. 5 and 6, it may be further concluded that, in the presence of a mobile PU and time-dependent fading channels, the reliable spectrum sensing (e.g., $P_D = 100\%$) requires an RMSE smaller than 20 m and a channel estimation MSE less than 0.1.

C. Different Sample Size M

In the second experiment, the effects from different sample sizes on the sensing and localization performance are studied. First, we note from Fig. 8 that the localization RMSE of a mobile PU will be promoted by increasing the sample size M. For example, when an $SNR = 15$ dB is concerned, the RMSE is 5.34 m if M is set to 50, while it will be significantly decreased to 1.65 m when $M = 200$. Second, a similar trend will be observed from the MSE curves of channel estimation. From Fig. 9, the MSE of channel estimation is 0.0638 when M is set to 50, while it may be decreased to 0.0069 when $M = 200$. That is easy to follow, i.e., with more independent samples, the degree of freedom of the accumulated observation will be then increased, leading to the more accurate estimation of hidden parameters.

The total correct probability P_D of the new DS scheme with different M is demonstrated by Fig. 10. It is seen from numerical results that the correct probability P_D will be promoted with the increasing of the sample size M. When the sample size is increased from $M = 50$ to $M = 100$, a rough detection gain of 2.5 dB may be achieved. Note that, however, an increased sample size M indicates a prolonged sensing time and also a

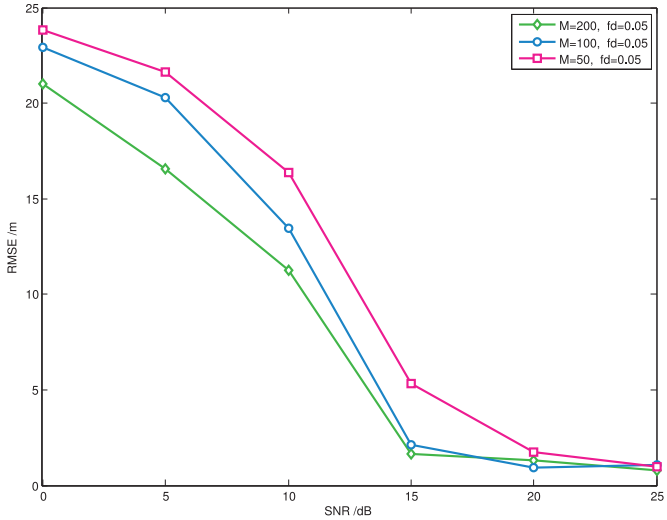

Fig. 8. Localization RMSE of PU under different sample size M.

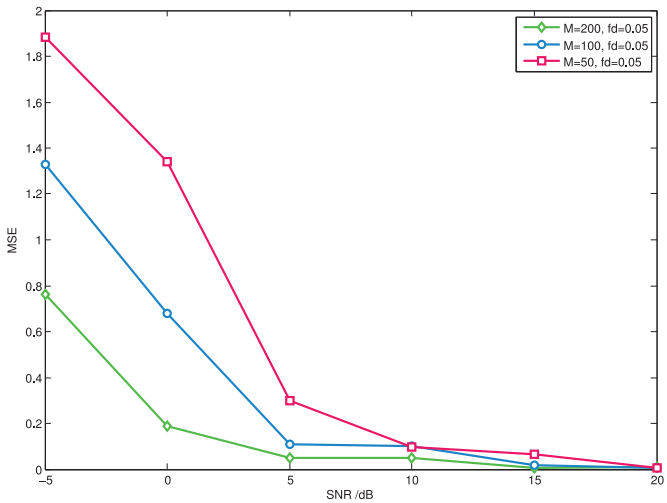

Fig. 9. Channel estimation MSE of the PU-SU link under different sample size M.

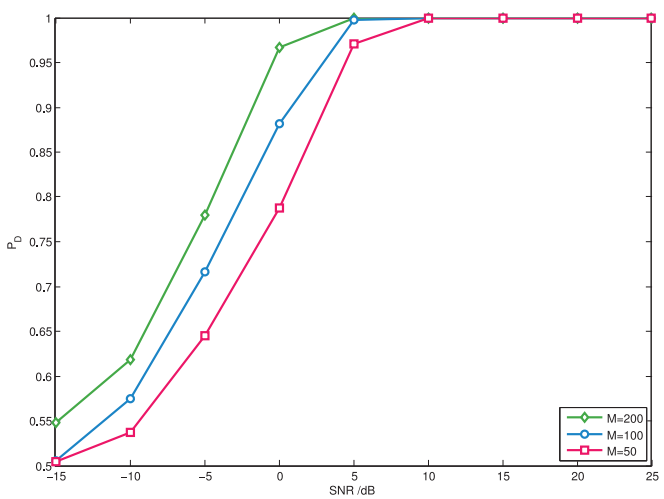

Fig. 10. Total correct probability under different sample sizes M.

higher complexity. As a consequence, the compromise should be made in the realistic designing.

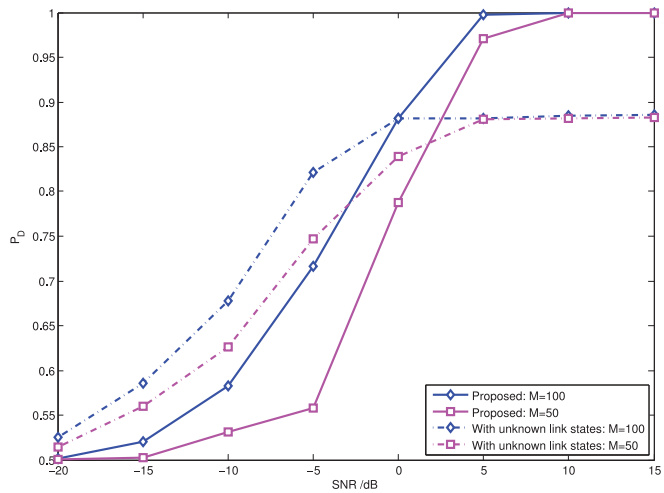

Fig. 11. Total correct probability with unknown PU's positions and the time-varying fading channels. Here, we configure $f_d = 0.05$.

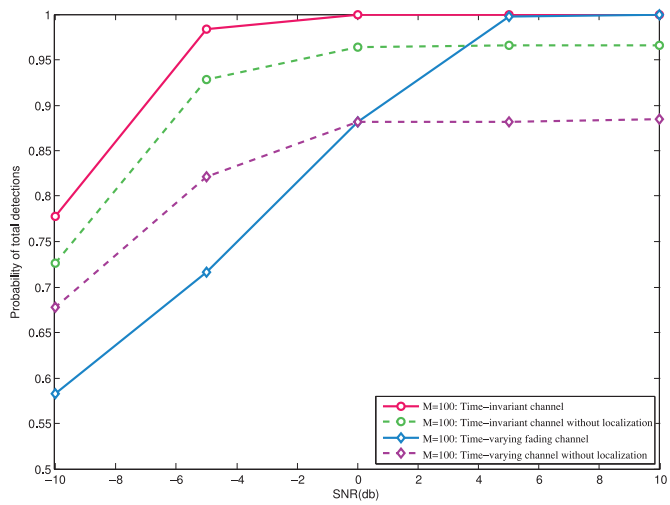

Fig. 12. Sensing performance in time-invariant fading channels and time-varying fading channels. In the simulation, we configure $f_d = 0.05$.

D. Comparative Analysis

We firstly investigate the common ED scheme without tracking PU's mobile positions and time-correlated flat fading channels. In the experiment, the PU's locations change dynamically with time, yet we may only know its expected location $\bar{\mathbf{l}} = \mathsf{E}\{\mathbf{l}_n\}$. For the varying flat-fading channels, we can also obtain the expectations of K fading gains, i.e., $\bar{\alpha}_r = \mathsf{E}\{\alpha_{n,r}\} = \int_{\alpha_{n,r}} \alpha_{n,r} f(\alpha_{n,r}) d\alpha_{n,r} \simeq \sum_{r=0}^{K-1} \rho_{k,r} \mathrm{A}_{k,r}$. Thus, the likelihood densities $p(\mathbf{z}_n | \{\bar{a}_r\}, \bar{\mathbf{l}}, s_n)$ will be evaluated and the MAP decision is made. It is found from Fig. 11 that, when these two link states become unknown to SUs, the sensing performance will be dramatically deteriorated by the resulting information uncertainty. Although the expectations of unknown link states lead to more robust sensing performance in low SNRs (e.g., <0 dB), the total correct detection probability can only be converged to 0.88, which is known as the SNR wall. Thus, the motivation of our suggested sensing algorithm can be demonstrated. I.e., it is of significance to acquire PU's mobile positions and time-varying fading gains when detecting the availability of spectrum.

In order to investigate the robustness of the DS scheme, we further obtain the sensing performance in time-invariant channels. Simulation results are shown by Fig. 12. By assuming the prior knowledge on the expectation of PU's location, i.e., $\overline{\mathbf{l}} = \mathsf{E}\{\mathbf{l}_n\}$, a benchmark method is studied in the absence of the time-varying fading, which similarly relies on the non-coherent energy observation and the likelihood densities $p(\mathbf{z}_n|\overline{\mathbf{l}}, s_n)$. We can see from the numerical results that, due to the additional information uncertainty introduced by the time-varying fading channels, the spectrum sensing process will be affected significantly. Compared with the time-invariant scenarios, the sensing performance may be degraded by about 7 dB under variant fading channel. Meanwhile, the advantage of the proposed DS scheme is fully demonstrated whether the flat-fading channel is time-varying or not. It can indeed promote the sensing performance remarkably and avoid the SNR wall of the sensing performance by acquiring the dynamic locations of a mobile PU.

V. Conclusion

The user mobility and the resulting time-varying fading are two main stumbling-blocks for spectrum sensing of the DSS-based next-generation communications, which renders the path-loss and fading gains time-dependent and, therefore, poses great difficulties to existing non-coherent sensing techniques. The DS scheme, which is designed to address a mixed detection and estimation problem, provides a promising approach to spectrum sensing in more challenging space-time doubly selective fading scenarios. Relying on a Bayesian MAP criterion, the new DS algorithm is implemented recursively and a simplified numerical scheme is suggested to alleviate the complexity. Some adaptive mechanisms are integrated to further enhance the performance, e.g., the observation accumulation and the AHE. It is demonstrated from numerical simulations that the proposed algorithm will track PU's locations and time-varying fading gains accurately. Such acquired link states information, which has been utilized to realize the spectrum sensing effectively, may be of also significance to further performance enhancement (e.g., power control and spatial transmissions of SUs). Future works may include the experimental validations. The new DSM and the proposed DS scheme can be extended to other scenarios, which, therefore, put an insight into spectrum sensing and provide a brand-new idea for future spectrum awareness communications.

References

[1] C. X. Wang, F. Haider, X. Q. Gao, X. H. You, Y. Yang, D. F. Yuan, H. Aggoune, H. Haas, S. Fletcher, and E. Hepsaydir, "Cellular architecture and key technologies for 5G wireless communication networks," *IEEE Commun. Mag.*, vol. 52, no. 2, pp. 122–130, 2014.

[2] J. G. Andrews, S. Buzzi, W. Choi, S. Hanly, A. Lozano, A. C. K. Soong, and J. Z. C. Zhang, "What will 5G be?," *IEEE J. Sel. Areas Commun.*, vol. 32, no. 16, pp. 1065–1082, 2014.

[3] M. Mueck, W. Jiang, G. L. Sun, H. W. Cao, E. Dutkiewicz, and S. Choi, "Novel Spectrum Usage Paradigms for 5G," White Paper, IEEE Technical Committee on Cognitive Networks SIG CR in 5G, Nov. 2014.

[4] H. J. Zhang, X. L. Chu, W. S. Guo, and S. Y. Wang, "Coexistence of Wi-Fi and heterogeneous small cell networks sharing unlicensed spectrum," *IEEE Commun. Mag.*, vol. 53, no. 3, pp. 158–164, 2015.

[5] R. Di Taranto, S. Muppirisetty, R. Raulefs, D. Slock, T. Svensson, and H. Wymeersch, "Location-aware communications for 5G networks: How location information can improve scalability, latency, and robustness of 5G," *IEEE Signal Process. Mag.*, vol. 31, no. 6, pp. 102–112, Nov. 2014.

[6] H. Celebi and H. Arslan, "Utilization of location information in cognitive wireless networks," *IEEE Wireless Commun.*, vol. 14, no. 4, pp. 6–13, 2007.

[7] J. Ma, G. Y. Li, and B.-H. Juang, "Signal processing in cognitive radio," *Proc. IEEE*, vol. 97, no. 5, pp. 805–823, May 2009.

[8] Y. H. Zeng and Y. C. Liang, "Eigenvalue-based spectrum sensing algorithms for cognitive radio," *IEEE Trans. Commun.*, vol. 57, no. 5, pp. 1784–1793, 2009.

[9] E. Axell, G. Leus, E. G. Larsson, and H. V. Poor, "Spectrum sensing for cognitive radio: State-of-the-art and recent advances," *IEEE Signal Process. Mag.*, vol. 29, no. 3, pp. 101–116, May 2012.

[10] L. Lu, X. W. Zhou, U. Onunkwo, and G. Y. Li, "Ten years of cognitive radio technology," *EURASIP J. Wireless Commun. Netw.*, vol. 28, pp. 1–16, 2012.

[11] F. F. Digham, M. S. Alouini, and M. K. Simon, "On the energy detection of unknown signals over fading channels," in *Proc. IEEE Int. Conf. Commun. (ICC)*, Anchorage, AK, USA, May 2003, vol. 5, pp. 3575–3579.

[12] B. Li, M. W. Sun, X. F. Li, A. Nallanathan, and C. L. Zhao, "Energy detection based spectrum sensing for cognitive radios over time-frequency doubly selective fading channels," *IEEE Trans. Signal Process.*, vol. 63, no. 2, pp. 402–417, Jan. 2015.

[13] B. Li, S. H. Li, Y. J. Nan, A. Nallanathan, C. L. Zhao, and Z. Zhou, "Deep sensing for next-generation dynamic spectrum sharing: More than detecting the occupancy state of primary spectrum," *IEEE Trans. Commun.*, vol. 63, no. 7, pp. 2442–2457, 2015.

[14] I. Guvenc, I and C. C. Chong, "A survey on TOA based wireless localization and NLOS mitigation techniques," *IEEE Commun. Surveys Tuts.*, vol. 3, no. 11, pp. 107–124, 2009.

[15] L. Taponecco, A. A. Damico, and U. Mengali, "Joint TOA and AOA estimation for UWB localization applications," *IEEE Trans. Wireless Commun.*, vol. 10, no. 7, pp. 2207–2217, 2011.

[16] M. Kazemi, B. Mahboobi, and M. Ardebilipour, "Performance analysis of simultaneous location and power estimation using WLS method for cognitive radio," *IEEE Commun. Lett.*, vol. 15, no. 10, pp. 1062–1064, Oct. 2011.

[17] H. Celebi and H. Aralan, "Cognitive positioning systems," *IEEE Trans. Wireless Commun.*, vol. 6, no. 12, pp. 4475–4483, 2007.

[18] J. G. Proakis, *Digital Communications*, 3rd ed. Singapore, Singapore: McGraw-Hill, 1995.

[19] J. Wang, J. H. Chen, and D. Cabric, "Cramér-Rao bounds for joint RSS/DOA-based primary user localization in cognitive radio networks," *IEEE Trans. Wireless Commun.*, vol. 12, no. 3, pp. 1363–1375, 2013.

[20] B. Li, S. H. Li, A. Nallanathan, and C. L. Zhao, "Deep sensing for future spectrum and location awareness 5G communications," *IEEE J. Sel. Areas Commun.*, vol. 33, no. 7, pp. 1331–1344, 2015.

[21] B. Li, Z. Zhou, and A. Nallanathan, "Joint estimation based spectrum sensing for cognitive radios in time variant flat fading channel," in *Proc. IEEE Global Commun. Conf. (Globecom)*, Atlanta, GA, USA, Dec. 2013, pp. 3212–3217.

[22] B. Vujitic, N. Cackov, and S. Vujitic, "Modeling and characterization of traffic in public safety wireless network," in *Proc. Int. Symp. Perform. Evaluat. Comput. Telecommun. Syst.*, Edinburgh, U.K., Jul. 2005, pp. 213–223.

[23] P. Sadeghi, R. Kennedy, P. Rapajic, and R. Shams, "Finite-state Markov modeling of fading channel: A survey of principles and applications," *IEEE Signal Process. Mag.*, vol. 25, no. 5, pp. 57–80, 2008.

[24] B. Sklar, "Rayleigh fading channel in mobile digital communication systems part I: Characterization," *IEEE Commun. Mag.*, vol. 35, no. 7, pp. 90–100, 1997.

[25] H. S. Wang and N. Moayeri, "Finite-state Markov channel: A useful model for radio communication channels," *IEEE Trans. Veh. Technol.*, vol. 44, no. 1, pp. 163–171, 1995.

[26] W. B. Davenport, Jr. and W. L. Root, *An Introduction to the Theory of Random Signals and Noise*. New York, NY, USA: IEEE Press, 1958.

[27] T. Camp, J. Boleng, and V. Davies, "A survey of mobility models for Ad Hoc network research," *Wireless Commun. Mobile Comput.*, vol. 2, no. 5, pp. 483–1502, 2002.

[28] P. I. Bratanov, "User mobility modeling in cellular communications networks," Vienna University of Technology, 1999.

[29] Y. C. Liang, K. C. Chen, G. Y. Li, and P. Mahonen, "Cognitive radio networking and communications: An overview," *IEEE Trans. Veh. Technol.*, vol. 60, no. 7, pp. 3386–3407, Sep. 2009.
[30] M. S. Arulampalam *et al.*, "A tutorial on particle filters for online nonlinear/non-Gaussian Bayesian tracking," *IEEE Trans. Signal Process.*, vol. 50, no. 2, pp. 174–188, 2002.
[31] R. Mahler, *Statistical Multisource Multi-Target Information Fusion*. Norwood, MA, USA: Artech House, 2007.
[32] B. Ristic, B.-T. Vo, B.-N. Vo, and A. Farina, "A tutorial on Bernoulli filters: Theory, implementation and applications," *IEEE Trans. Signal Process.*, vol. 61, no. 13, pp. 3406–3430, 2013.
[33] B. T. Vo, B. N. Vo, and A. Cantoni, "Bayesian filtering with random finite set observations," *IEEE Trans. Signal Process.*, vol. 56, no. 4, pp. 1313–1326, 2008.
[34] B. Ristic and J. Sherrah, "Bernoulli filter for joint detection and tracking of an extended object in clutter," *IET Radar, Sonar Navig.*, vol. 7, no. 1, pp. 26–35, 2013.
[35] P. M. Djuric, J. H. Kotecha, J. Q. Zhang, Y. F. Huang, T. Ghirmai, M. F. Bugallo, and J. Miguez, "Particle filtering," *IEEE Signal Process. Mag.*, vol. 20, no. 5, pp. 19–38, 2003.
[36] J. Borwein and P. Borwein, *Pi and the AGM: A Study in Analytic Number Theory and Computational Complexity*. New York, NY, USA: Wiley, 1987.
[37] W. Zhang, R. K. Mallik, and K. B. Letaief, "Cooperative spectrum sensing optimization in cognitive radio networks," in *Proc. IEEE Int. Conf. Commun. (ICC)*, Beijing, China, May 19–23, 2008, pp. 3411–3415.
[38] S. K. Zheng, P. Y. Kam, Y. C. Liang, and Y. H. Zeng, "Spectrum sensing for digital primary signals in cognitive radio: A Bayesian approach for maximizing spectrum utilization," *IEEE Trans. Wireless Commun.*, vol. 12, no. 4, pp. 1536–1276, 2013.

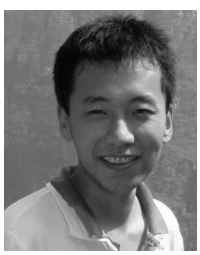

Bin Li received the Bachelor's degree in electrical information engineering from Beijing University of Chemical Technology (BUCT) in 2007, the Ph.D. degree in communication and information engineering from Beijing University of Posts and Telecommunications (BUPT) in 2013. He joined BUPT since 2013, as a lecture of the School of Information and Communication Engineering (SCIE). His current research interests are focused on statistical signal processing algorithms for wireless communications, e.g., ultra-wideband (UWB), wireless sensor networks, millimeter-wave (mm-Wave) communications and cognitive radios (CRs). He has published more than 60 journal and conference papers. He received 2011 ChinaCom Best Paper Award, 2010 and 2011 BUPT Excellent Ph.D. Student Award Foundation. He serves as the Co-Chair of the Technical program Committee of the Signal Processing for Communications Symposium of the 2016 IEEE International Conference on Computing, Networking and Communications (IEEE-ICNC'16).

Jia Hou received his B.S. degree in communication engineering from Wuhan University of Technology in 2000, China, M.S. and Ph.D. degrees in information communication from Chonbuk National University, Korea, in 2002 and 2005, respectively. He was the post-doctoral research fellow and the invited professor in Chonbuk National University, Korea, from April 2005 to April 2007.

And now he is the associate professor in Soochow University, Suzhou, China. His main research interests are Signal Processing, sequences, error coding and space time signal processing. He has published more than sixty research papers in international journals and conferences proceedings.

Xiaofan Li (M'10) is the Deputy Chief Engineer of the State Radio monitoring center and Testing Center (SRTC) Shenzhen Lab, received her B.S. degree and Ph.D. degree from Beijing University of Posts and Telecommunication (BUPT) in 2007 and 2012. From 2010 to 2011, she was a visiting Ph.D. student in University of Washington. She has involved in nearly 10 national foundation projects. Her research interests include interference analysis among different radio systems, testing method and technology on radio equipments, cooperative transmission, cognitive radio, internet of things, radio management policy, etc.

Yijiang Nan received his B.S. degree in communication engineering from Tianjin University in 2013, China. He is currently pursuing the masters degree at Beijing University of Posts and Telecommunications (BUPT). His research interests include cognitive radios and statistical signal processing.

Arumugam Nallanathan (S'97–M'00–SM'05) is a Professor of Wireless Communications in the Department of Informatics at King's College London (University of London). He served as the Head of Graduate Studies in the School of Natural and Mathematical Sciences at King's College London, 2011–2012. He was an Assistant Professor in the Department of Electrical and Computer Engineering, National University of Singapore from August 2000 to December 2007. His research interests include 5G Technologies, Millimeter wave communications, Cognitive Radio and Relay Networks. In these areas, he co-authored more than 250 papers. He is a co-recipient of the Best Paper Award presented at the 2007 IEEE International Conference on Ultra-Wideband (ICUWB'2007). He is an IEEE Distinguished Lecturer. He is an Editor for IEEE TRANSACTIONS ON COMMUNICATIONS and IEEE TRANSACTIONS ON VEHICULAR TECHNOLOGY. He was an Editor for IEEE TRANSACTIONS ON WIRELESS COMMUNICATIONS (2006–2011), IEEE WIRELESS COMMUNICATIONS LETTERS and IEEE SIGNAL PROCESSING LETTERS. He served as the Chair for the Signal Processing and Communication Electronics Technical Committee of IEEE Communications Society, Technical Program Co-Chair (MAC track) for IEEE WCNC 2014, Co-Chair for the IEEE GLOBECOM 2013 (Communications Theory Symposium), Co-Chair for the IEEE ICC 2012 (Signal Processing for Communications Symposium), Co-Chair for the IEEE GLOBECOM 2011 (Signal Processing for Communications Symposium), Technical Program Co-Chair for the IEEE International Conference on UWB 2011 (IEEE ICUWB 2011), Co-Chair for the IEEE ICC 2009 (Wireless Communications Symposium), Co-Chair for the IEEE GLOBECOM 2008 (Signal Processing for Communications Symposium) and General Track Chair for IEEE VTC 2008. He received the IEEE Communications Society SPCE outstanding service award 2012 and IEEE Communications Society RCC outstanding service award 2014.

Chenglin Zhao received the Bachelor's degree in radio-technology from Tianjin University in 1986, and the Master's degree in circuits and systems from Beijing University of Posts and Telecommunications (BUPT) in 1993, and the Ph.D. degree in communication and information system from Beijing University of Posts and Telecommunications, in 1997. At present, he serves as a Professor in Beijing University of Posts and Telecommunications, Beijing, China. His research is focused on emerging technologies of short-range wireless communication, cognitive radios, 60 GHz millimeter-wave communications.